Draft version December 23, 2020
Typeset using LaTeX default style in AASTeX62

ANALYTIC STABILITY MAPS OF UNKNOWN EXOPLANET COMPANIONS FOR IMAGING PRIORITIZATION

Carlos Gascon,[1,2] Dmitry Savransky,[3,4] and Miquel Sureda[1]

[1] *ESEIAAT, Polytechnic University of Catalonia, Terrassa, Barcelona 08222, Spain*
[2] *School of Mathematics and Statistics, Polytechnic University of Catalonia, Barcelona, Barcelona 08028, Spain*
[3] *Sibley School of Mechanical and Aerospace Engineering, Cornell University, Ithaca, NY 14853, USA*
[4] *Carl Sagan Institute, Cornell University, Ithaca, NY 14853, USA*

ABSTRACT

Identifying which systems are more likely to host an imageable planet can play an important role in the construction of an optimized target list for future direct imaging missions, such as the planned Coronagraph Instrument (CGI) technology demonstration for the **Nancy Grace Roman Space Telescope**. For single-planet systems, the presence of an already detected exoplanet can severely restrict the target's stable region and should therefore be considered when searching for unknown companions. To do so, we first analyze the performance and robustness of several two-planet stability criteria by comparing them with long-term numerical simulations. We then derive the necessary formulation for the computation of (a, R) analytic stability maps, which can be used in conjunction with depth-of-search grids in order to define the stable-imageable region of a system. The dynamically stable completeness (i.e., the expected number of imageable and stable planets) can then be calculated via convolution with the selected occurrence grid, obtaining a metric that can be directly compared for imaging prioritization. Applying this procedure to all the currently known single-planet systems within a distance of 50 pc, we construct a ranked target list based on the **CGI's** predicted performance and SAG13 occurrence rates. **Finally, we evaluate the importance of considering the radial velocity data from past Doppler surveys in order to rule out entire regions of our parameter space where, if a planet existed, it would have certainly been detected by previous RV observations.**

Keywords: methods: analytical - planets and satellites: dynamical evolution and stability - planets and satellites: detection

1. INTRODUCTION

While indirect detection methods, such as radial velocity and transit photometry, have been the main source of exoplanetary information to date, direct imaging has emerged as a challenging but highly desirable technique, providing unique information regarding the atmospheric structure and chemical composition of exoplanets (Konopacky et al. 2013). In this context, space-based direct imaging instruments, such as the **Nancy Grace Roman Space Telescope's** Coronagraph Instrument (CGI), will enable the expansion and better characterization of the known population of exoplanets. Given the high cost and complexity of space observatories, detailed and extensive planning is required in order to ensure the successful execution of the mission. In particular it is essential to create optimized target lists by identifying which systems are more likely to host imageable planets.

Garrett et al. (2017) addressed this problem by defining the depth-of-search grids in the (a, R) space, where the value of each bin represented the probability of detecting a planet with semi-major axis a and radius R. The resultant imageable region was obtained according only to the instrument's performance and capabilities, allowing for the estimation of the expected number of detected planets (i.e., total completeness) by convolution with an assumed grid of occurrence rates. A similar procedure can be used to evaluate the observability of previously discovered planets. This provides two potential sources of targets: stars with no known planets where a new planet is likely to be observable, and stars with known planets that could potentially be imaged with a new instrument. There remains, however, a third category: stars with known planets that are *not* observable with proposed instrumentation, but which may harbor additional planets that could be imaged. There also exists an overlapping population between the second and third

categories, composed of targets where the known planet could be imaged, but we would also be interested in detecting additional, unknown, companions via imaging.

When searching for additional exoplanets in already known single-planet systems, the gravitational effect of the existing body can severely restrict the target's stable region and must therefore be taken into account. For instance, let us consider a nearby star with a large imageable region and a massive highly eccentric planet in the center of such a region. In this context, most of the detectable area would be chaotic due to the known planet's presence, consequently reducing the probability of detecting a stable unknown companion in a system which a priori seemed a valuable target. In general, for any system the following question is naturally raised: How many stable unknown companions could an instrument detect? We seek to answer this question in an accurate but computationally inexpensive manner, in order to rapidly identify which targets have a higher probability of hosting an additional planet and discard those systems where no unknown companions could be detected. To do so, in Section 2 we begin by describing several two-planet stability criteria and comparing them with long-term numerical simulations. In Section 3 we derive the necessary expressions for the conditional density function of the outer pericenter to inner apocenter ratio (ρ) and the angular momentum deficit (C), which will be essential for the computation of analytic stability maps presented in Section 4.

Finally, in Section 5 we make use of these results, together with depth-of-search and occurrence grids, in order to obtain the expected number of imageable and stable planets for a given target. We conclude by presenting 213 currently known single-planet systems within 50 parsecs of the Earth, ranked according to the **CGI's** predicted performance and the Study Analysis Group 13 (SAG13) occurrence rates. **This ranking, when coupled with updated Doppler sensitivities for potential targets, could aide researchers working on any CGI participating science program that follows the initial technology demonstration phase of the instrument, and would potentially greatly expand the sample of targets observed by both Doppler spectroscopy and direct imaging.**

2. ANALYTIC STABILITY CRITERIA FOR TWO-PLANET SYSTEMS

Unlike systems with three or more planets, the stability of two-planet systems can be analytically characterized via several different criteria. One of the main results was obtained by Marchal & Bozis (1982), who extended the notion of Hill stability to the general three-body problem and showed that certain initial conditions can preclude close encounters between the outer planet and the inner bodies. Based on this result, Gladman (1993) found that two planets in initially circular and coplanar orbits are Hill stable if

$$a_2 - a_1 > 2\sqrt{3} R_H \,, \tag{1}$$

where

$$R_H = \left(\frac{m_1 + m_2}{3 M_\star} \right)^{1/3} \frac{a_1 + a_2}{2} \tag{2}$$

is the mutual Hill radius, $M_\star$ is the mass of the central star, a_i are the semi-major axes of the planet orbits, m_i are the planetary masses, and the subscripts 1 and 2 refer to the inner and outer planet, respectively. It is important to note, however, that long-term interactions between planets in Hill stable orbits could still ultimately lead to the ejection of the outer planet or the collision of the inner planet with the star (i.e., Lagrange instability). From another perspective, Wisdom (1980) applied the resonance overlap criterion to the coplanar and circular restricted three body problem. By studying the region around a planet where first order mean motion resonances (MMRs) overlap, the author found that a test particle with semi-major axis a would experience chaotic motion if

$$\frac{|a - a_p|}{a_p} < C_{\rm w} \mu_p^{2/7} \,, \tag{3}$$

where $C_{\rm w}$ is a constant value, a_p is the semi-major axis of the planet and $\mu_p = m_p / M_\star$ is the mass ratio between the planet and the star. Although originally Wisdom obtained a theoretical value of $C_{\rm w} = 1.33$, Duncan et al. (1989) presented a numerically-derived estimate of $C_{\rm d} = 1.57$. For the case of two massive planets in circular orbits, Deck et al. (2013) extended Wisdom's criterion and predicted that all orbits should be chaotic if

$$\frac{a_2 - a_1}{a_1} < 1.46 \epsilon^{2/7} \,, \tag{4}$$

where $\epsilon = (m_1 + m_2)/M_\star$ is the planets-to-star mass ratio. Deck et al. (2013) also developed a similar expression for non-circular configurations, only applicable, however, **when the weighted eccentricity satisfies $\boldsymbol{\sigma \approx e_1 + e_2 \gtrsim 1.33\epsilon^{3/7}}$ and eccentricities are low enough that overlap of resonances of second order and beyond are negligible**. For arbitrary eccentricities, several criteria have been proposed (Giuppone et al. 2013; Petrovich 2015; Laskar & Petit 2017; Petit et al. 2017; Petit et al. 2018), which we will divide into two generic categories depending on whether the criterion is based on the outer pericenter to inner apocenter ratio (ρ) or the angular momentum deficit ($\boldsymbol{C}$).

2.1. *Criteria based on the Outer Pericenter to Inner Apocenter ratio*

As demonstrated by Petrovich (2015), most of the proposed two-planet stability criteria for arbitrary eccentricities can be expressed as a boundary of the ratio between the pericenter of the outer planet and the apocenter of the inner planet, here denoted by

$$\rho = \frac{a_2(1-e_2)}{a_1(1+e_1)}\,, \tag{5}$$

where e_1 and e_2 are the corresponding eccentricities. Giuppone et al. (2013) developed an extended crossing orbit criterion by adding and subtracting Wisdom's overlap region (Wisdom 1980, Equation 3) to the outer pericentric and inner apocentric distances, respectively. They also took into account the effect of the difference in the longitudes of the pericenter $\Delta\bar{\omega}$ and proposed stability limits for the case of aligned ($\Delta\bar{\omega} = 0°$) and anti-aligned ($\Delta\bar{\omega} = 180°$) initial orbits. By studying the stability limits of a test planet around a known and existing planet, they presented the following criterion for the anti-aligned configuration

$$\rho > \begin{cases} \dfrac{1}{1-\delta} & a_2 = a_k \\ 1+\delta & a_1 = a_k\,, \end{cases} \tag{6}$$

where a_k is the known planet's semi-major axis and $\delta = 1.57(\mu_1^{2/7} + \mu_2^{2/7})$. Here we will make use of the modification proposed by Hadden & Lithwick (2018), where they employ $\delta = 1.46\epsilon^{2/7}$ in accordance to the results of Deck et al. (2013). Alternatively, Petrovich (2015) approached the problem numerically by performing long-term integrations for a large number of planetary systems and a wide range of eccentricities and inclinations. They found ρ to be the single parameter that best described the stability boundary and presented the following empirical criterion

$$\rho > 1.15 + 2.4\left[\max(\mu_1,\mu_2)^{1/3}\right]\left(\frac{a_2}{a_1}\right)^{1/2}. \tag{7}$$

2.2. *Criteria based on the Angular Momentum Deficit*

Considering the secular approximation of a planetary system, Laskar & Petit (2017) developed an alternative stability criterion based on the conservation of the angular momentum deficit (AMD). Following the definition of Laskar (2000), the AMD (C) is given by the difference between the norm of the angular momentum of an equivalent circular and coplanar system and the norm of the real system's angular momentum, which for a system of n_p planets is

$$C = \sum_{j=1}^{n_p} \Lambda_j(1 - \sqrt{1-e_j^2}\cos i_j)\,, \tag{8}$$

where i_j is the relative inclination, $\Lambda_j = m_j\sqrt{GM_\star a_j}$ and G is the gravitational constant. For a two-planet system, Laskar & Petit (2017) defined the relative angular momentum deficit as

$$\mathscr{C} = \frac{C}{\Lambda_2} = \gamma\sqrt{\alpha}(1 - \sqrt{1-e_1^2}\cos i_1) + (1 - \sqrt{1-e_2^2}\cos i_2)\,, \tag{9}$$

where $\alpha = a_1/a_2$ represents the semi-major axis ratio and $\gamma = m_1/m_2$ is the mass ratio. In this context, they obtained the minimum relative AMD which allowed for planetary collisions, referred to as the collisional critical AMD $\left(C_c^{\mathrm{C}}\right)$. Consequently, since the AMD is conserved at all orders (Laskar & Petit 2017), the impossibility of collisions between the two planets is ensured if the initial relative AMD is bounded as

$$\mathscr{C} < C_c^{\mathrm{C}}(\alpha,\gamma). \tag{10}$$

This condition can be extended to multiple planet systems by analyzing the AMD-stability of every pair of adjacent planets, as well as the innermost planet and the star. Furthermore, Agnew et al. (2018) compared the previous criterion with numerical simulations over a large number of known systems and concluded that the AMD-stability is a reliable tool for determining the stability of planetary systems. In order to take into account the effect of mean motion resonances (MMR) ignored by the secular theory, Petit et al. (2017) proposed a new derivation of the first-order MMR overlap criterion in the AMD framework. They refined the criteria presented by Wisdom (1980) and Deck et al. (2013) by deriving a more global expression, for which they then associated a new critical AMD $\left(C_c^{\rm MMR}\right)$. Since it only makes sense to apply the first-order MMR criterion when α is close to 1, they combined this with the previous collision criterion $\left(C_c^{\rm C}\right)$ and defined the following piece-wise critical AMD (Petit et al. 2017)

$$\mathscr{C} < C_c(\alpha,\gamma,\epsilon) = \begin{cases} C_c^{\rm C}(\alpha,\gamma) & \alpha < \alpha_R(\epsilon,\gamma) \\ C_c^{\rm MMR}(\alpha,\gamma,\epsilon) & \alpha > \alpha_R(\epsilon,\gamma)\,, \end{cases} \tag{11}$$

where α_R represents the semi-major axis ratio at which $C_c^{\rm C} = C_c^{\rm MMR}$. For lower values of α, the collisional criterion becomes stricter and consequently more useful.

Continuing their work in the AMD framework, Petit et al. (2018) generalized the stability criterion proposed by Gladman (1993) and defined the Hill stability AMD criterion

$$\mathscr{C} < C_c^{\rm H}(\alpha,\gamma,\epsilon) = \gamma\sqrt{\alpha} + 1 - (1+\gamma)^{3/2}\sqrt{\frac{\alpha}{\gamma+\alpha}\left(1 + \frac{3^{4/3}\epsilon^{2/3}\gamma}{(1+\gamma)^2}\right)}, \tag{12}$$

where $C_c^{\rm H}$ is defined as the Hill critical AMD. As this expression was obtained as an approximation of the criterion from Marchal & Bozis (1982), Petit et al. (2018) compared both criteria and proved that Equation (12) is accurate for the typical range of values of ϵ and still valid for very large or small planetary mass ratios (γ).

2.3. *Numerical Simulations and Criteria Comparison*

To assess the performance and robustness of the criteria described above, we performed several numerical simulations in order to study and compare their behaviour over a wide range of parameters. Specifically, we added a test planet to two known single-planet systems (HD 154345 and HD 114613) and analyzed the long-term stability of the resultant two-planet systems. The stellar parameters and the orbital elements of the known planet, denoted by the subscript k, were extracted from the NASA Exoplanet Archive[1] and can be found summarized in Table 1. For simplicity, all systems were assumed to be coplanar and the existing planet's mass was considered to be the minimum value $m_k \sin I$, where I is the system's inclination with respect to the line of sight. The remaining unknown parameters, such as the longitude of the ascending node or the initial mean anomaly, were all set to zero. For each system, we then constructed two different types of stability maps.

1. *(a, e) stability map:* regular grid with 70 logarithmically spaced semi-major axis bins and 40 linearly spaced eccentricity bins. The ranges of a and e were selected taking into the account the extension of the chaotic region around the known planet's semi-major axis a_k. The test planet's mass m was constant through the whole grid, being fixed in a different value depending on the system. In particular, for the system HD 114613 a mass of 1 $M_{\rm J}$ was employed, while a smaller value was used in the case of HD 154345. On the other hand, the argument of periastron $\omega \in [0, 2\pi]$ was always randomly generated.

2. *(a, m) stability map:* regular grid with 70 semi-major axis bins and 40 mass bins, both logarithmically spaced. The range of values of a and m was determined considering the imageable region of the system with the **CGI**. In this case, the test planet's eccentricity e was constant through the whole grid, being fixed in a different value depending on the system. In the case of the system HD 154345, a nearly circular value was used, while a higher eccentricity was assigned to the test planet in the system HD 114613. Finally, ω was again randomly generated.

The particular values employed for every system and stability map are presented in Table 1. For each bin, we integrated the corresponding two-planet system using the Leapfrog integrator implemented in the REBOUND package

[1] The required orbital parameters where retrieved from the NASA Exoplanet Archive (https://exoplanetarchive.ipac.caltech.edu) on 2019 June 8.

Table 1. Stellar and Planetary Parameters

Target Star			Known Planet				(a, e) map			(a, m) map		
Name	Distance	$M_\star$	a_k	e_k	$m_k \sin I$	ω_k	a	e	m	a	e	m
	(pc)	($M_\odot$)	(AU)		(M_J)	(°)	(AU)		(M_J)	(AU)		(M_J)
HD 154345	18.294	0.71	4.21	0.04	0.82	0[a]	[2, 12]	[0, 0.5]	0.1	[1.5, 25]	0.05	[0.067, 134.45]
HD 114613	20.295	1.27	5.34	0.458	0.357	196	[1.5, 20]	[0, 0.5]	1	[1.5, 25]	0.1	[0.067, 134.45]

[a]The argument of periapsis w_k of the planet HD 154345 b was unknown and consequently set to zero.

NOTE—The (a, m) grid was ranged taking into account the imageable region of each system, which was assumed to be approximately the same in both cases. In particular, the limiting values of m correspond to a planetary radius R between 4 and 17 $R_\oplus$.

(Rein & Liu 2012). The simulations were run for 10^9 yr with a timestep of $T_1/50$, where T_1 is the orbital period of the innermost planet. Integrations were terminated if the two planets approached one another within one mutual Hill radius (Equation 2), or if a planet reached an astrocentric distance of either 5×10^{-3} or 250 AU.

Figure 1 shows the resultant stability maps for a nearly circular configuration (HD 154345) and a highly eccentric system (HD 114613). In general, we observe that Petrovich's criterion shows the most conservative boundaries, appearing to be too pessimistic in the first case and slightly more appropriate for large eccentricities. In contrast, the complete AMD stability limit (Equation 11) falls inside the chaotic region in most cases and will be consequently discarded for the purposes of the following sections. Similarly to Giuppone's criterion, the Hill AMD boundaries offer an acceptable necessary condition for stability and could therefore be used as a more optimistic alternative. In particular, we remark how the Hill AMD stability condition accurately delimits the earliest chaotic orbits in both (a, e) maps, likely corresponding to the region where planetary close encounters occur. Hence, the remaining instabilities outside these boundaries may be the result of ejections or collisions between the inner planet and the star, which by definition are not taken into account in the Hill criterion. Furthermore, the HD 114613 (a, m) stability map shows a pronounced increase in the Hill stability limits as the test planet's mass decreases, disagreeing with other criteria and the numerical simulations. Such behavior, which essentially increases the predicted unstable region, becomes more significant for high eccentricities and can be related to the Hill stability's strong dependence on the planetary mass ratio γ for non-circular configurations (Deck et al. 2013). We must keep in mind that the Hill stability criterion from Marchal & Bozis (1982) cannot be directly applied to the elliptic restricted three body problem and therefore should not be used when one of the planetary masses is close to zero. Nonetheless, given that in most cases the **CGI-imageable** region only covers high-mass planets, the Hill AMD can still be considered a valid criterion in the following sections. Regarding the test planet's mean motion resonances with the existing planet, we note how for the nearly circular case, the stable resonant lines are more predominant and extend up to larger values of e and m, while being less numerous and significant in the high-eccentricity system.

3. DERIVATIONS

Let us consider a coplanar, three-body system consisting of a central star of mass $M_\star$, and two orbiting planets, where the mass and orbital elements of one of the planets (a_k, e_k, m_k) are known. The remaining planet is unknown, and its parameters (a, e and m) will be consequently treated as random variables. In particular, the eccentricity e will follow a Rayleigh distribution with parameter σ (i.e. mean eccentricity $\mu_e = \sigma\sqrt{\pi/2}$), while the semi-major axis a and the planet's mass m will have a joint probability density function $f_{\bar{a},\bar{m}}(a, m)$ representative of the population of interest. With this setup, for fixed values of a and m, the integral of the conditional density function of both the AMD (C) and the outer pericenter and inner pericenter ratio (ρ) can be easily solved. As will be shown in Section 4, this result will be essential for the computation of the analytic stability maps and the prioritization of planetary systems for followup imaging.

3.1. *ρ Conditional Density Function*

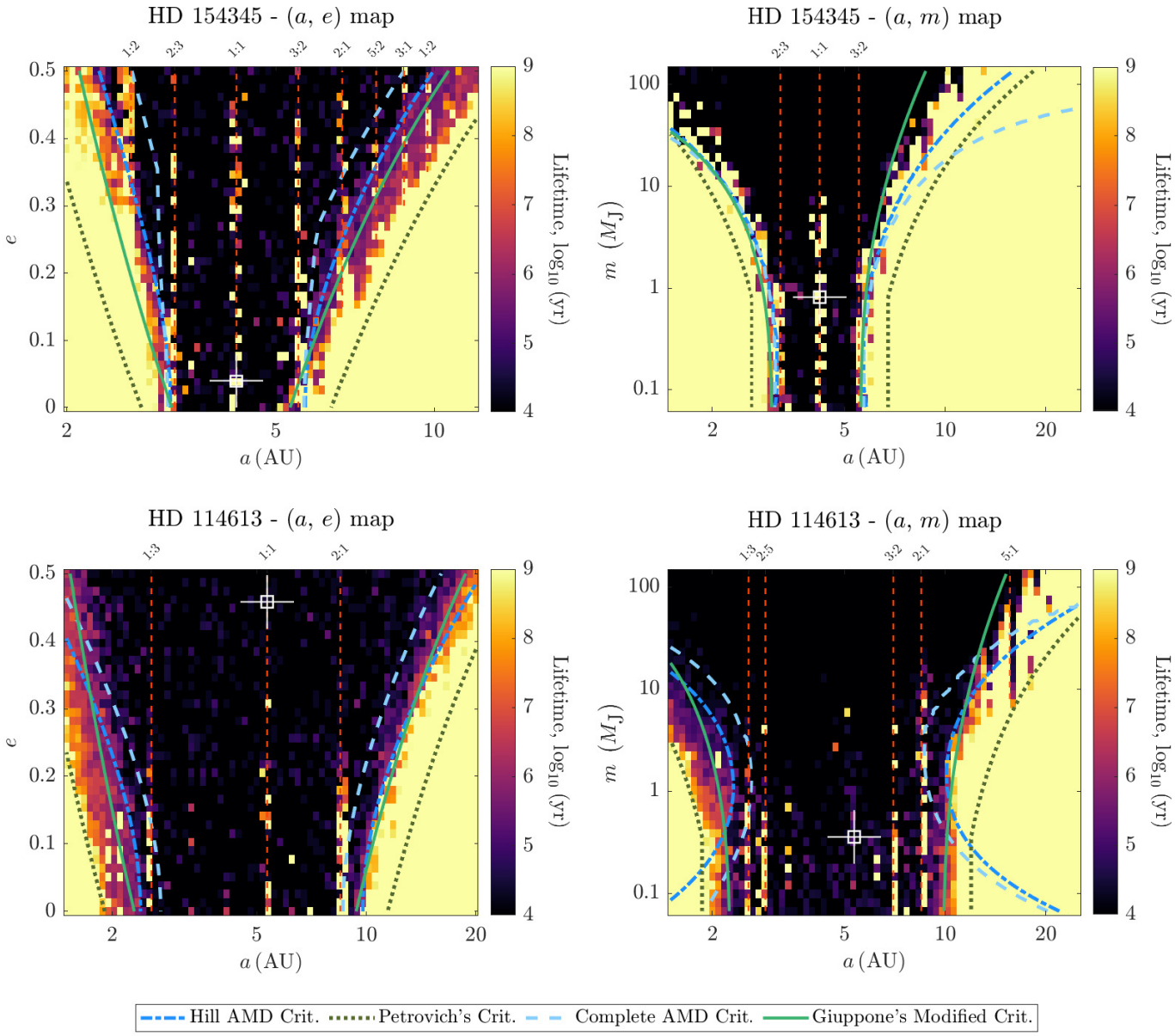

Figure 1. Numerical stability maps for the nearly circular system HD 154345 (top) and high eccentricity system HD 114613 (bottom), compared to the stability boundaries given by the criteria specified in the legend. The white marker indicates the position of the existing planet and the red dashed lines indicate low-order mean motion resonances with the known planet.

Making use of Equation (5), the outer pericenter to inner apocenter ratio can be rewritten as

$$\rho = g_\rho(e, a) = \begin{cases} \dfrac{q_k}{a(1+e)} & a < a_k \\ \dfrac{a(1-e)}{Q_k} & a > a_k \,, \end{cases} \tag{13}$$

where $q_k = a_k(1 - e_k)$ and $Q_k = a_k(1 + e_k)$ are, respectively, the known planet's pericenter and apocenter. For a fixed semi-major axis a, we observe that $\rho = g_\rho(e \mid a)$ is a univariate function only dependent on e. Consequently, the inverse function $h_\rho = g_\rho^{-1}(\rho \mid a)$ is directly obtained by isolating the eccentricity in Equation (13)

$$e = h_\rho(\rho \mid a) = \begin{cases} \dfrac{q_k - a\rho}{a\rho} & a < a_k \\ \dfrac{a - Q_k\rho}{a} & a > a_k \,. \end{cases} \tag{14}$$

For simplicity, we will omit the conditional notation in $h_\rho(\rho)$ from here on out, since we are primarily interested in evaluating all expressions for a given value of a. Taking the derivative of Equation (14) with respect to ρ, we get

$$\left|\frac{dh_\rho}{d\rho}(\rho)\right| = \begin{cases} \dfrac{q_k}{a\rho^2} & a < a_k \\ \dfrac{Q_k}{a} & a > a_k\,. \end{cases} \tag{15}$$

Using Equations (14) and (15), the ρ conditional density function is then given by

$$f_{\bar{\rho}|\bar{a}}(\rho \mid a) = f_{\bar{e}}(h_\rho(\rho)) \left|\frac{dh_\rho}{d\rho}(\rho)\right|\,, \tag{16}$$

where $f_{\bar{e}}(e)$ is the density function of the eccentricity, assumed to be Rayleigh distributed. For fixed values of a and m, the probability of having a stable configuration, denoted by $S_\rho(a,m)$, is obtained by integrating Equation (16) over the region defined by the specific ρ stability criterion used:

$$S_\rho(a,m) = \int_{\rho_{c,l}}^{\rho_{c,u}} f_{\bar{\rho}|\bar{a}}(\rho \mid a)d\rho = F_{\bar{e}}(h_\rho(\rho_{c,u})) - F_{\bar{e}}(h_\rho(\rho_{c,l}))\,, \tag{17}$$

where $\rho_{c,l}(a,m)$ and $\rho_{c,u}(a,m)$ are the lower and upper limit, respectively. Given our assumptions, the integral can be simply calculated as the difference between the Rayleigh cumulative distribution function $F_{\bar{e}}(e)$ evaluated at the limiting eccentricities $h_\rho(\rho_{c,u})$ and $h_\rho(\rho_{c,l})$. Substituting h_ρ from Equation (14) yields the solution

$$S_\rho(a,m) = \begin{cases} -\exp\left(\dfrac{-1}{2\sigma^2}\left(\dfrac{q_k - a\rho}{a\rho}\right)^2\right)\Bigg|_{\rho_{c,l}}^{\rho_{c,u}} & a < a_k \\ -\exp\left(\dfrac{-1}{2\sigma^2}\left(\dfrac{a - Q_k\rho}{a}\right)^2\right)\Bigg|_{\rho_{c,l}}^{\rho_{c,u}} & a > a_k\,. \end{cases} \tag{18}$$

The majority of currently available exoplanet data for **CGI-imageable** planets has been obtained from radial velocity (RV) surveys. While transit photometry currently leads in the total number of exoplanet discoveries, most of these (primarily due to Kepler and the K2 mission) are too distant for imaging with the next generation of space-based coronagraphic instruments, and the **CGI** in particular. While we expect this to change with the Transiting Exoplanet Survey Satellite (TESS) and other surveys, for now, the true mass m_k of the majority of known exoplanets of interest remains undetermined, and only the minimum mass $m_{k,min} = m_k \sin I$ is known. In these cases, we rewrite the probability integral (17) as $S_\rho(a,m,m_k)$ and we introduce the system's inclination $I \in [0,\pi)$ as a new random variable with a sinusoidal probability density function $f_{\bar{I}}(I) = \sin(I)/2$. We can then take into account the effect of the known planet's mass uncertainty by using Equation (18) and defining

$$S_\rho^{'}(a,m) = \int_0^\pi S_\rho\left(a, m, \frac{m_{k,min}}{\sin(I)}\right) f_{\bar{I}}(I)\,\mathrm{d}I\,. \tag{19}$$

For the stability criteria based on ρ, Equations (18) and (19) will be directly used for the computation of analytic stability maps. Similarly, we now derive the equivalent formulation for the angular momentum deficit C.

3.2. *C Conditional Density Function*

For a two-planet system ($n_p = 2$), Equation (8) can be written as

$$C = g_C(e,a,m) = K + \Lambda(1 - \sqrt{1-e^2})\,, \tag{20}$$

where $K = \Lambda_k(1 - \sqrt{1-e_k^2})$ accounts for the known planet AMD contribution. For fixed values of a and m, $\Lambda = m\sqrt{GM_\star a}$ is completely defined and therefore $C = g_C(e \mid a,m)$ is only a function of e. The inverse function $g_C^{-1}(C \mid a,m)$, which we will denote as h_C, is then obtained by solving Equation (20) for the eccentricity

$$e = h_C(C \mid a,m) = \sqrt{1 - \left(\frac{\Lambda - C + K}{\Lambda}\right)^2}\,, \tag{21}$$

where again the conditional notation will be dropped for simplicity. Since the inverse function must have the range $e = h_C(C) \in [0, 1)$, the derivative

$$\left|\frac{dh_C}{dC}(C)\right| = \frac{1}{\Lambda}\left(\frac{\sqrt{1-h_C^2(C)}}{h_C(C)}\right) \tag{22}$$

is well defined except for the case $C = K$ (i.e. $h_C(C) = 0$). However, this singularity is naturally solved when the expression of the conditional density function is simplified

$$f_{\bar{C}|\bar{a},\bar{m}}(C \mid a, m) = f_{\bar{e}}(h_C(C))\left|\frac{dh_C}{dC}(C)\right| = \frac{\sqrt{1-h_C^2(C)}}{\Lambda\sigma^2}\exp\left(\frac{-h_C^2(C)}{2\sigma^2}\right), \tag{23}$$

where the formula of the Rayleigh probability density function for $f_{\bar{e}}(e)$ has been used. Following the same procedure as in Section 3.1, for certain values of $C_{c,l}(a, m)$ and $C_{c,u}(a, m)$ determined by the specific AMD stability criterion used, the integral of the conditional density function is

$$S_C(a, m) = \int_{C_{c,l}}^{C_{c,u}} f_{\bar{C}|\bar{a},\bar{m}}(C \mid a, m)\,\mathrm{d}C = F_{\bar{e}}(h_C(C_{c,u})) - F_{\bar{e}}(h_C(C_{c,l}))\,. \tag{24}$$

Making use of Equation (21), the analytic solution is then given by

$$S_C(a, m) = -\exp\left(\frac{1}{2\sigma^2}\left(\left(\frac{\Lambda - C + K}{\Lambda}\right)^2 - 1\right)\right)\Bigg|_{C_{c,l}}^{C_{c,u}}. \tag{25}$$

As described in the previous subsection, in the case of systems with an undetermined planetary mass m_k, we redefine the probability of having a stable configuration as

$$S_C^{'}(a, m) = \int_0^{\pi} S_C\left(a, m, \frac{m_{k,min}}{\sin(I)}\right) f_{\bar{I}}(I)\,\mathrm{d}I\,. \tag{26}$$

Although a more detailed and consistent single-planet ranking is described in Section 5, a first approach relies on the definition of the a, m and C (or ρ) joint probability density function

$$f_{\bar{a},\bar{m},\bar{C}}(a, m, C) = f_{\bar{a},\bar{m}}(a, m) \cdot f_{\bar{C}|\bar{a},\bar{m}}(C \mid a, m)\,. \tag{27}$$

By choosing the appropriate limits of integration which approximately define the imageable region, together with the stability boundaries of C, a rapid estimation of the probability of detecting a stable planet can be computed as

$$\int_{m_l}^{m_u}\int_{a_l}^{a_u} f_{\bar{a},\bar{m}}(a, m)\left(\int_{C_{c,l}}^{C_{c,u}} f_{\bar{C}|\bar{a},\bar{m}}(C \mid a, m)\,dC\right)\mathrm{d}a\,\mathrm{d}m\,, \tag{28}$$

where the term in the inner parentheses has already been analytically solved, simplifying the calculation to a double integral. Equation (28), which can be equivalently derived for ρ, can be used to discard those systems with barely any stable imageable region or to obtain a first imaging prioritization in a fast and computationally inexpensive manner.

4. ANALYTIC STABILITY MAPS

Following the previous assumptions and derivations, in this section we compute the analytic stability maps which will allow us to rapidly characterize the stable region of a particular single-planet system. Essentially, these maps consist of a regular grid with 100 semi-major axis bins and 100 mass bins, both logarithmically spaced and ranged around the system's imageable region. For a particular pair (a, m), the value of the corresponding bin represents the probability of having a stable configuration according to the specific criterion used. For the systems where the known planet's mass m_k is completely determined, the stability maps are built using Equations (18) and (25), depending on the type of criterion used. On the other hand, if only $m_k \sin I$ is known, Equations (19) and (26) are employed. To illustrate this, we select the empirical criterion presented by Petrovich (2015), since it appears to give the most conservative and

consistent boundaries according to the results from Section 2.3. Based on the critical ρ from inequality (7), we define the lower limit of integration

$$\rho_{c,l}^{\mathrm{P}}(a,m) = \begin{cases} 1.15 + 2.4\left[\max(\mu,\mu_k)^{1/3}\right](a_k/a)^{1/2} & a < a_k \\ 1.15 + 2.4\left[\max(\mu_k,\mu)^{1/3}\right](a/a_k)^{1/2} & a > a_k\,. \end{cases} \tag{29}$$

In general, given that we are only considering elliptical orbits (i.e., $e \in [0,1)$), the outer pericenter to inner apocenter ratio must have a range $\rho \in (g_\rho(1,a), g_\rho(0,a)]$ and therefore, $\rho_{c,l}$ should always be adjusted to the range of values of ρ. That is, if $\rho_{c,l}(a,m) < g_\rho(1,a)$ then $\rho_{c,l}(a,m) = g_\rho(1,a)$, and equivalently if $\rho_{c,l}(a,m) > g_\rho(0,a)$ then $\rho_{c,l}(a,m) = g_\rho(0,a)$. Furthermore, the expression of $g_\rho(0,a)$ allows us to set the upper limit as

$$\rho_{c,u}(a) = g_\rho(0,a) = \begin{cases} \dfrac{q_k}{a} & a < a_k \\ \dfrac{a}{Q_k} & a > a_k\,. \end{cases} \tag{30}$$

In addition, we will also construct stability maps using Giuponne's criterion (Giuppone et al. 2013, Equation 6) and the Hill AMD criterion (Petit et al. 2018, Equation 12), which will serve as an alternative for ranking planetary systems. In the first case, the lower limit of integration is directly given by Equation (6) and can be written as

$$\rho_{c,l}^{\mathrm{G}}(a,m) = \begin{cases} \dfrac{1}{1 - 1.46\epsilon^{2/7}} & a < a_k \\ 1 + 1.46\epsilon^{2/7} & a > a_k\,, \end{cases} \tag{31}$$

while the upper limit $\rho_{c,u}$ is again given by Equation (30). On the other hand, assuming that the stellar mass $M_\star$ is known, the Hill critical AMD is only a function of the semi-major axis and mass ratios. From the definition of $C_c^{\mathrm{H}}(\alpha,\gamma)$ given in Equation (12), we then derive the upper limit of integration as

$$C_{c,u}(a,m) = \begin{cases} \Lambda_k\, C_c^{\mathrm{H}}(a/a_k, m/m_k) & a < a_k \\ \Lambda\, C_c^{\mathrm{H}}(a_k/a, m_k/m) & a > a_k\,, \end{cases} \tag{32}$$

for which again the range of values of $C \in [g_C(0,a,m), g_C(1,a,m))$ should be taken into consideration. In particular, the lower limit of integration is defined and given by $C_{c,l}(a,m) = g_C(0,a,m) = K$.

We demonstrate this procedure by generating the (a, m) analytic stability maps of the single-planet systems HD 154345 and HD 114613 (Figure 2). Since none of the system's inclinations are known, we make use of Equations (19) and (26), together with the limits of integration presented above. The mean eccentricity for the Rayleigh distribution is taken to be $\mu_e = 0.225$ (Moorhead et al. 2011) and the required orbital parameters, as well as the range of values of a and m, are as in Table 1. **In the most favourable case where the unknown planet follows instead a circular orbit, the stable region would be delimited by the gray dashed curves in Figure 2, which essentially correspond to the 0 contour lines.** Furthermore, we can easily build (a, R) stability maps by considering instead a set of logarithmically spaced planetary radius R bins and applying the previous expressions to the corresponding planetary masses. For each value of R, the related mass m is predicted using the FORECASTER best-fit density model (Chen & Kipping 2016), originally composed of linear segments (in log-log space) of the form

$$R = 10^{C + \log_{10}(m) S}\,, \tag{33}$$

where C and S are fit coefficients defined in four mass intervals: Terran, Neptunian, Jovian and Stellar Worlds. Due to inclusion of many tidally locked, inflated Jupiters in the model, the original results tend to overestimate the radius for Jovian-size planets, and so we slightly modify the initial fit by moderating the transition between the Saturn and Jupiter mass-radius points. Specifically, the Neptunian Worlds segment is adjusted to end at the Saturn mass-radius point, from which a new fit is added as a straight line (in the log-log space) until the Jupiter mass-radius point. Moreover, the Jovian segment is corrected to be a constant Jupiter radius value ranging from 1 Jupiter Mass through 0.08 Solar Masses. The Terran and Stellar Worlds, on the other hand, remain unchanged. The resultant values of C and S, for Earth mass and radius units, are shown in Table 2. It is important to note that we are not suggesting that

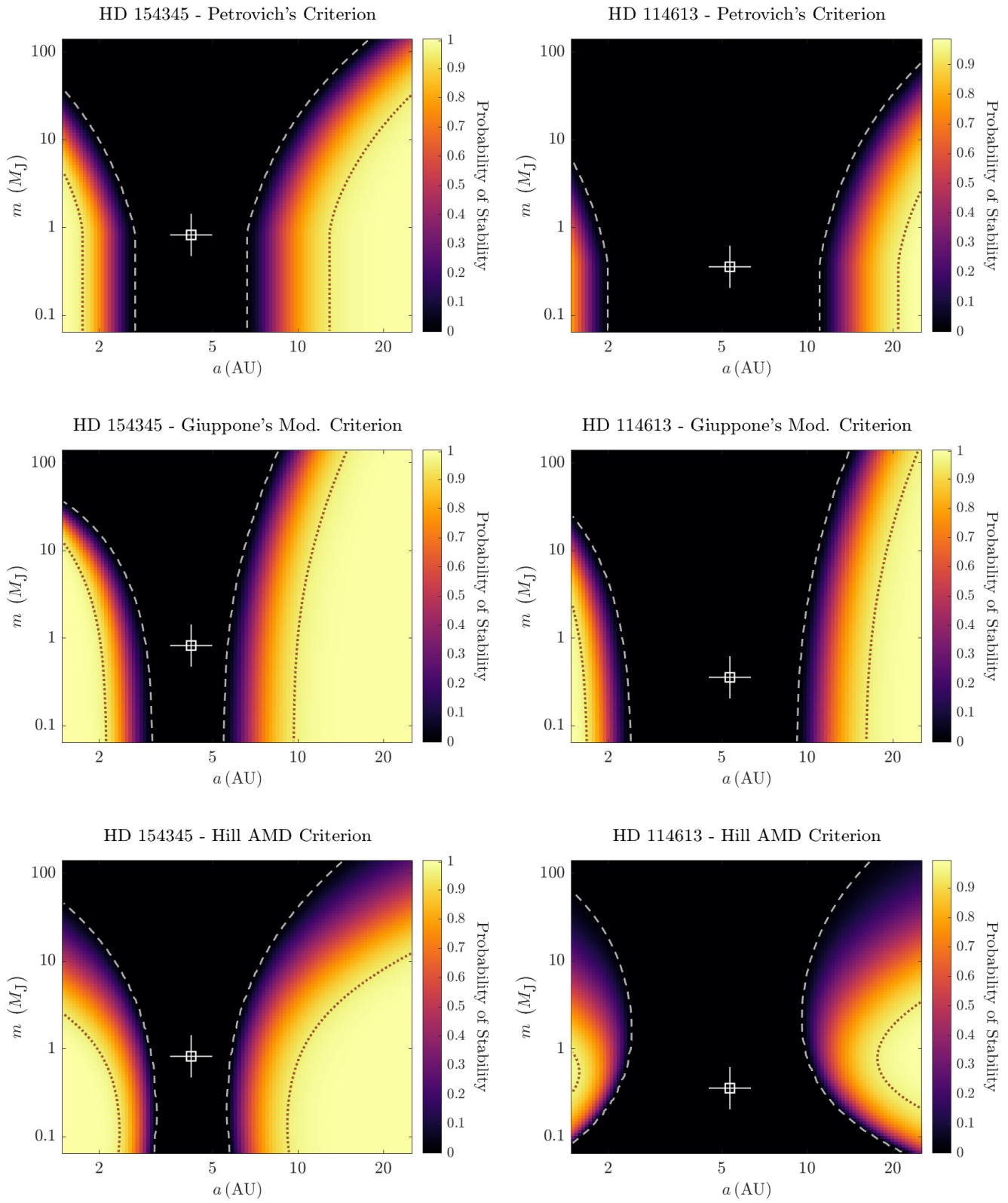

Figure 2. (Modified Figure) Analytic stability maps for the systems HD 154345 (left column) and HD 114613 (right column), using Petrovich's empirical criterion (top row), Giuppone's modified criterion (middle row) and the Hill AMD criterion (bottom row). **The white marker indicates the position of the existing planet, the dashed gray line delimits the stable region in the circular case and the dotted brown curve is the 0.95 contour line.**

Table 2. C and S parameters of the FORECASTER modified fit

m ($M_\oplus$)	C	S
$m \leq 2.04$	0.00346053	0.279
$2.04 < m \leq 95.16$	-0.06613329	0.50376436
$95.16 < m \leq 317.828407$	0.48091861	0.22725968
$317.828407 < m \leq 26635.6863$	1.04956612	0
$m > 26635.6863$	-2.84926757	0.881

our modified fit is in any way more 'correct' than the original FORECASTER model. Rather, as we are focusing on only the larger orbits amenable to direct imaging, we wish to avoid generating planetary mass objects of greater than 1 Jupiter radius, which are expected to be exceedingly rare at the relevant separations. As the original fit also passes quite near the Saturn mass-radius point, we chose to explicitly incorporate Saturn's density in our modification.

While the general procedure and calculations presented in the coming sections rely on the use of a Rayleigh distribution for the eccentricity, we note that the results from Moorhead et al. (2011) were obtained from a sample consisting mostly of intermediate and low-mass planets, and are therefore potentially applicable to only certain regions of the parameter space considered. The range of masses defined by the imageable region directly depends on the system's distance, and therefore, the adequacy of a particular distribution will be essentially determined by the region involved. For instance, in the case of the closest and more interesting targets where lower mass planets are included, the use of the distribution from Moorhead et al. (2011) is certainly convenient. Furthermore, the assumption of a Rayleigh distribution allows for the derivation of a simple and easy to compute expression, which might be more helpful when analyzing large target lists. Alternatively, in the case of the higher-mass regions also explored in our study, the use of, for instance, the Beta distribution proposed by Kipping (2013) may also be a suitable alternative worth considering. To do so, in Figure 3, we reproduce two sample cases assuming that the unknown planet's eccentricity follows a Beta(a, b) distribution with parameters $a = 0.867$ and $b = 3.03$, while the systems and stability criteria remain the same. As we can see, despite certain differences regarding the spatial evolution of the probability of stability, the resulting stability maps bear a considerable resemblance to the figures obtained with the Rayleigh distribution, with only small variations in the overall results yielded by the complete analysis performed in the following sections.

5. SINGLE-PLANET SYSTEMS PRIORITIZATION

Having constructed the analytic stability maps, we now address the main purpose of this study by identifying which single-planet systems are more likely to host an additional, imageable planet. Basically, the proposed methodology consists of estimating and comparing the expected number of planets (i.e., occurrence rates) within each system's stable-imageable region defined in the (a, R) space. To do so, together with the stability maps obtained in Section 4, we shall make use of the following additional grids:

1. *Depth-of-search grid:* Given a particular system, we obtain its imageable region by computing the depth-of-search grids as defined by Garrett et al. (2017). For given values of a and R, the corresponding bin represents the conditional probability of detecting a hypothetically existing planet (i.e., completeness; Brown 2005) according to the considered instrument's design and capabilities. In particular, here we set the necessary optical parameters and contrast limits according to the **CGI's** inner and outer working angles and predicted contrast curve in the 575 nm imaging band. For planet photometry, we use the model grids from Batalha et al. (2018), which are interpolated to find the phase curves of various planets in reflected light.

2. *Occurrence grid:* In order to calculate the expected number of planets in a certain region, we build occurrence grids using the SAG 13 parametric fit for G-dwarfs. Similarly to Garrett & Savransky (2018), we translate the

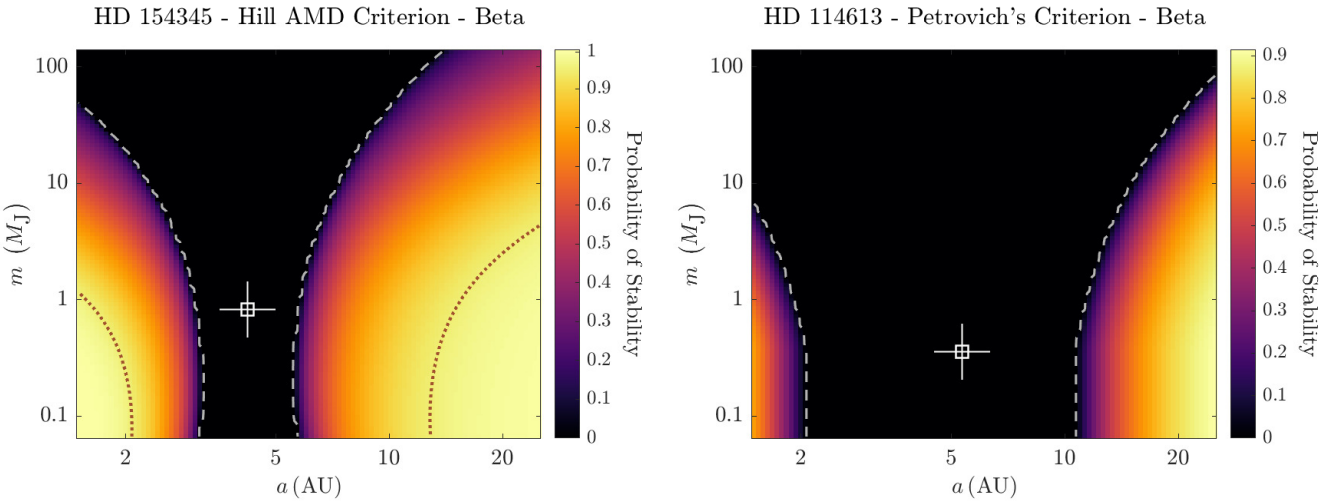

Figure 3. (New Figure) Analytic stability maps assuming the eccentricity follows a beta distribution, for the systems HD 154345 (left) and HD 114613 (right), using the Hill AMD and Petrovich's criterion, respectively. The white marker indicates the position of the existing planet, the dashed gray line delimits the stable region in the circular case and the dotted brown curve is the 0.95 contour line.

Table 3. (New Table) SAG13 parametric fit parameters.

$R\ (R_\oplus)$	Γ	α	β
$R < 3.4$	0.38	-0.19	0.26
$R \geq 3.4$	0.73	-1.18	0.59

original period-radius broken power law into the (a, R) space and we add an exponential decay term starting at $a_k = 10$ AU. **The resulting parametric model for the occurrence rate η is then given by**

$$\frac{\partial^2 \eta}{\partial R\, \partial a} = \Gamma_i R^{\alpha_i - 1} \left(2\pi \sqrt{\frac{a^3}{\mu}}\right)^{\beta_i - 1} \left(3\pi \sqrt{\frac{a}{\mu}}\right) \exp\left(-\left(\frac{a}{a_k}\right)^3\right),$$

where the values of the original SAG13 fit parameters Γ, α and β can be found in Table 3.

Given that the size of the imageable region strongly depends on the distance from the observer to the target star, all three grids are ranged according to each system's detection boundaries ($a_{\min}$, $a_{\max}$ and $R_{\min}$). This is intended to increase the accuracy of the results by only calculating stability around the imageable zone. In general, the maximum planetary radius is set to $R_{\max} = 17 R_\oplus$, since we only wish to consider bodies near the planetary mass regime. For the semi-major axis, the inner limit will be essentially determined by the minimum projected separation

$$a_{\min} = s_{\min} = IWA \cdot d\,, \tag{34}$$

where IWA is the telescope's inner working angle and d is the distance to the system. To find the maximum value of a, we consider the expression for the ratio of fluxes between the planet and the star (Brown 2005)

$$F_R = p\Phi\left(\beta\right)\left(\frac{R}{r}\right)^2, \tag{35}$$

where p and β are the planet's albedo and phase angle, respectively, Φ is the phase function and r is the distance between the planet and the star. For a particular value of R, the upper limit of the imageable region is characterized

by the maximum a such that the planet meets the instrument's obscurational and photometric constraints, determined by $s_{\min}$ and the expected mininum contrast $c_{\min}$. These values can be related to the upper boundary of the nonzero region of the completeness joint probability density function (Garrett & Savransky 2016) given by one of the solutions of

$$F(a \mid R) = c_{\min} - p\Phi\left[\sin^{-1}\left(\frac{s_{\min}}{a}\right)\right]\left(\frac{R}{a}\right)^2 = 0\,, \tag{36}$$

where r has been replaced by a, since the depth-of-search grids are defined assuming that $e = 0$ (Garrett et al. 2017). Since the width of the imageable region increases with R, the maximum semi-major axis $a_{\max}$ is consequently given by the upper bounding solution of the equation $F(a \mid R_{\max}) = 0$, where again $R_{\max}$ is the largest planetary radius considered. Having determined $a_{\min}$ and $a_{\max}$, we can finally obtain the minimum radius by isolating R in Equation (36) and calculating

$$R_{\min} = \min_{a\in(a_{\min},a_{\max})}\left\{\sqrt{\frac{a^2 c_{\min}}{p\Phi\left(\sin^{-1}\left(s_{\min}/a\right)\right)}}\right\}. \tag{37}$$

For each system, the product of the stability and depth-of-search grids yields the intersection between the stable and imageable regions, where the value of each bin gives the probability of detecting a stable planet of radius R and semi-major axis a. For instance, in Figure 4 we represent the resultant grids for the systems HD 154345 and HD 114613, using the Hill AMD and Petrovich's criteria respectively. In order to properly identify the limits of the nonzero regions, the bins with null probability are not coloured.

As expected, in both cases the size of the imageable region is clearly defined by the solutions to the equations presented above. Such limits, together with the estimated detection probability of each bin, are only a function of the distance to the system and the instrument's capabilities. In consequence, the resemblance between both depth-of-search grids can be directly related to the similar target distance (see Table 1), while also evidencing that the results ignore integration time constraints since there is no dependence on the magnitude of the star. Regarding the (a, R) stability maps, we first note a clear contrast between the extension of the unstable regions of both systems, essentially as a result of the difference in the orbital eccentricities of the existing planets and the stability criteria employed. Moreover, the use of the modified FORECASTER best-fit described in Section 4 results in a discontinuous increase in planetary mass occurring at 1 $R_{\rm J}$ ($\approx 11.2 R_\oplus$), causing the steep growth in the unstable region observed at that point. In general, the stable-imageable grid demonstrates how the depth-of-search is highly perturbed by the region where planets cannot exist due to instabilities, confirming that the presence of the known planet should be considered when optimizing the target selection. The sum over the intersection bins, normalized by the number of bins and multiplied by the grid area, yields what we refer to as the dynamically stable depth-of-search. This value has no dependence on the assumed planet population and only accounts for the considered instrument's performance and stability criterion. Finally, the convolution of the intersection region with the occurrence grid returns the desired estimate of the expected number of stable and imageable planets in the system (dynamically stable completeness), yielding a metric that can be directly used for imaging prioritization.

We apply this procedure to all 213 currently known single-planet systems within a distance of 50 pc, creating a ranking based on Petrovich's stability criterion and complemented by the results obtained with Giuppone's and the Hill AMD criteria (Appendix A). Naturally, the results show a clear dependence on the system's distance d, generally making the closest targets the most valuable. Nonetheless, we also note how some of the nearest stars present a lower dynamically stable completeness in comparison to farther targets with smaller imageable regions. This is clearly observed in Figure 6, where the stable completeness for every target analyzed and stability criteria used, as a function of the system's distance, is represented. As a result of the dependence of the imageable region on the distance to the system, the expected number of stable and imageable planets decreases along the horizontal axis. Those targets where the presence of the known planet has a greater effect present a lower stable completeness, consequently falling below the main tendency defined by the upper line. Comparing the results given by each stability criterion, we observe how Giuppone's criterion usually returns the highest completeness values, while Petrovich's and the Hill AMD criteria, in accordance with the behaviors observed in Section 2.3, tend to give more conservative results. Although we are focusing on the search of unknown companions, the systems where the already existing exoplanet falls inside the imageable region (such as HD 154345 or HD 114613) are still interesting targets, given that the majority of known exoplanets have been discovered with indirect detection techniques and still need to be directly imaged **in order to obtain spectral information, which will allow for modeling currently unknown properties such as their**

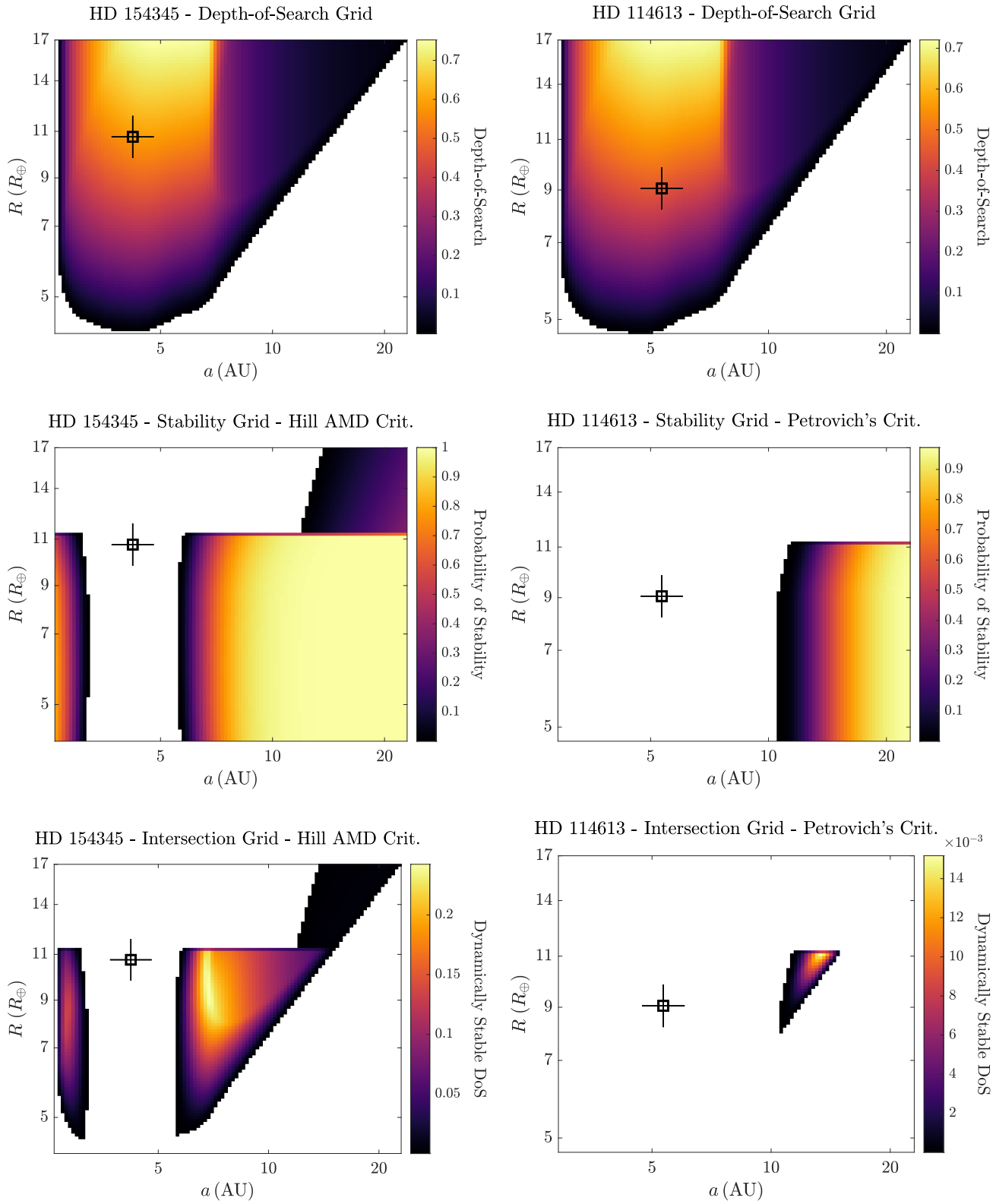

Figure 4. Depth-of-Search (top), Stability (middle) and Intersection (bottom) grids for the system HD 154345 using the Hill AMD criterion (left), and the system HD 114613 using Petrovich's criterion (right). The black marker indicates the position of the existing planet.

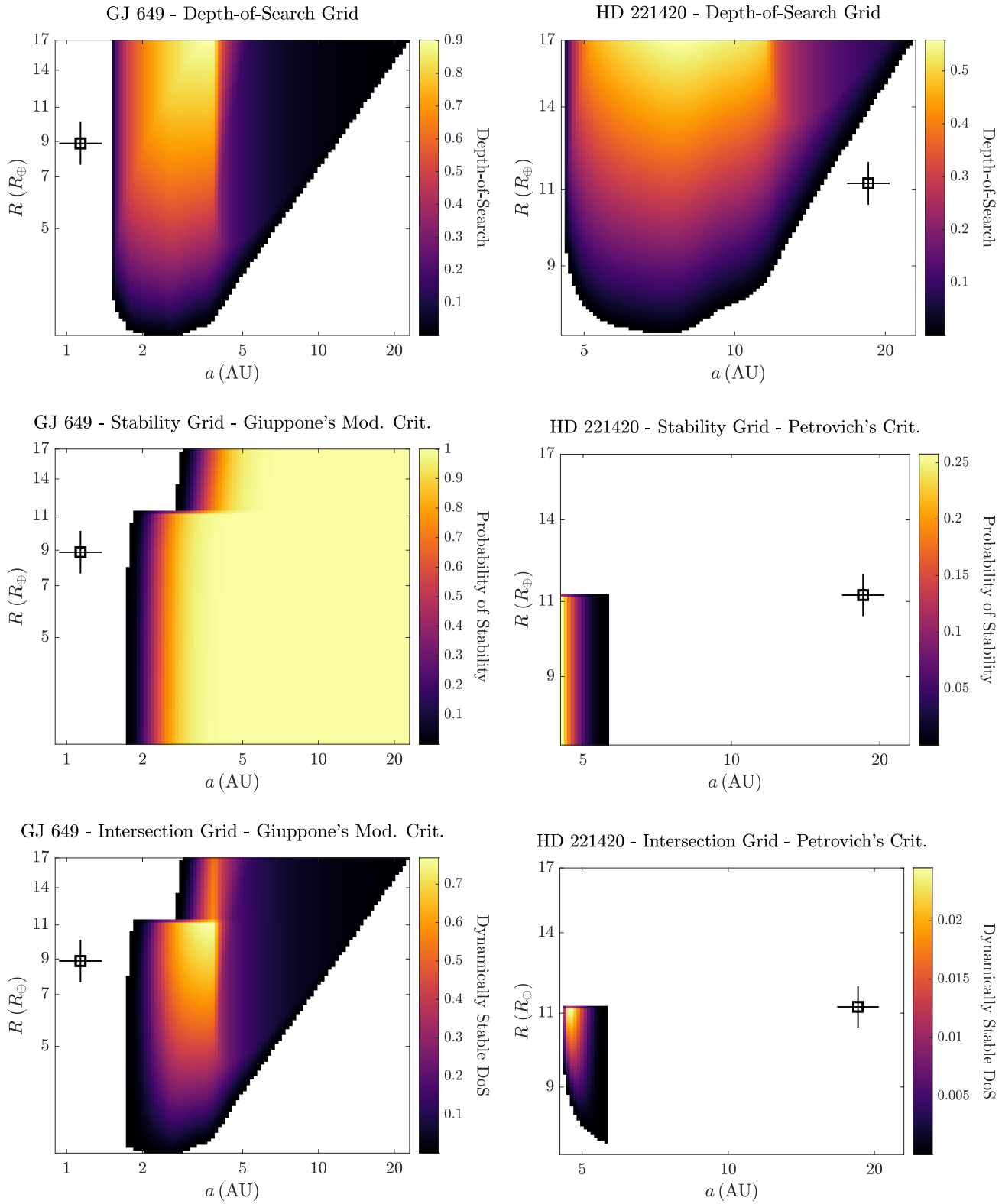

Figure 5. Depth-of-Search (top), Stability (middle) and Intersection (bottom) grids for the system GJ 649 using Giuppone's modified criterion (left), and the system HD 221420 using Petrovich's criterion (right). The black marker indicates the position of the existing planet.

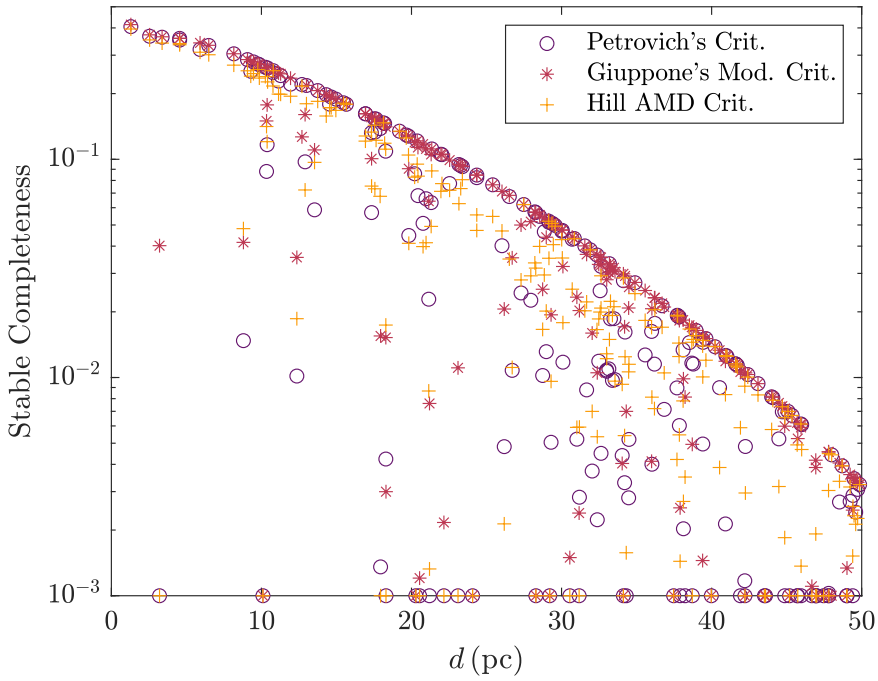

Figure 6. Stable completeness as a function of the system's distance. For all targets, the estimated number of imageable and stable planets according to each stability criterion is plotted. Completeness values below 10^{-3} are plotted over the horizontal axis.

atmospheric structure or chemical composition. In Figure 5 we present the resultant grids for the systems GJ 649 and HD 221420, where the existing planet is located outside the lower and upper limits of the imageable region, respectively. **These plots clearly demonstrate how the presence of the known planets, which are themselves unobservable with the assumed instrument, still impacts the likelihood of observing other potential planets in these systems.**

Furthermore, in order to complete our study, we should also take into account the radial velocity data obtained from past Doppler surveys. In this sense, the exploration and subsequent non-detection of additional planets in some of the targets considered may help us rule out entire regions of our parameter space where, if a planet existed, it would have certainly been detected by previous RV observations. To do so, we directly apply the results from Howard & Fulton (2016), where they use measurements at both Lick and Keck Observatories taken by the California Planet Survey in order to evaluate the probability of recovering an additionally injected synthetic RV signal simulating the presence of a planet of mass $m \sin I$ and semi-major axis a. In particular, for each target considered, they introduce 5000 synthetic planets uniformly distributed and apply an iterative planet search algorithm to attempt to detect the injected signals, ultimately obtaining a spatial distribution of the corresponding recovery rates. They apply this procedure to a target list containing 76 nearby stars, 6 of which were single-planet systems also present in our star sample. While repeating the recovery tests for the remaining 207 stars included in our target list is beyond the scope of this work, we can make use of the available calculations by combining our dynamically stable completeness maps with the results presented by Howard & Fulton (2016). Regarding the latter, due to the differences between the range of values employed in each study, we need to carefully translate the recovery rate distribution from Howard & Fulton (2016) into our parameter space and grid values. To do so, we build our adapted contour plots by linearly interpolating the recovery rates corresponding to the grid points falling inside their original range of values. On the other hand, for the higher planetary masses considered in the present study, we follow the vertical trend observed in the original contour plots and perform a uniform extrapolation of the recovery rates associated with the upper mass limits evaluated in Howard & Fulton (2016). This entire procedure is demonstrated in the left-hand plot of Figure 7, where the distribution of recovery rates for the system HD 3651, adapted to our parameter space and range of values, is represented. In particular,

Table 4. (New Table) Doppler corrected dynamically stable completeness.

Target		Known Planet			Stable Completeness			Doppler Corrected Completeness		
Name	Distance	a_k	e_k	$m_k \sin I$	Petrovich	Giuppone	Hill AMD	Petrovich	Giuppone	Hill AMD
	(pc)	(AU)		(M_J)	(Stability criteria)			(Stability criteria)		
HD 3651	11.14	0.295	0.645	0.228	0.22829	0.24871	0.19898	0.13682	0.13693	0.11859
51 Peg	15.47	0.053	0.013	0.472	0.18147	0.18147	0.18074	0.10399	0.10399	0.10399
tau Boo	15.66	0.049	0.011	4.32	0.17870	0.17870	0.17870	0.12827	0.12827	0.12827
70 Vir	17.91	0.481	0.399	7.416	0.13822	0.14952	0.06767	0.08031	0.08291	0.01935
HD 19994	22.54	1.305	0.063	1.37	0.07743	0.09913	0.07212	0.05941	0.06159	0.05799
eps Eri	3.21	3.39	0.702	1.55	0.00046	0.04020	0.00016	0.00043	0.03795	0.00000

the gray dashed line indicates the mass above which the results were uniformly extrapolated, while the lower values were linearly interpolated. Similarly, the equivalent (a, R) maps can be constructed (right-hand plot of Figure 7), where now the colour map represents the fraction of non-recovered planets, which we will refer to as Doppler insensitivity. In this sense, in the regions where the Doppler insensitivity decreases (i.e., the fraction recovered is high), an additional planet would have already been detected by past RV surveys and therefore the corresponding probability of finding a new companion is lower. Furthermore, by combining the resulting Doppler insensitivity maps with our stable-imageable regions in the (a, R) space, we can compute the Doppler corrected, dynamically stable completeness associated with the six single-planet systems considered, the values of which can be found in Table 4. As we can observe, the consideration of the radial velocity data reduces significantly the target's total completeness, consequently suggesting that, in future studies, a detailed Doppler analysis for the most interesting targets would be needed in order to improve and complement our prioritization.

While the target ranking presented in Appendix A is certainly incomplete without the addition of Doppler insensitivity for all of the tabulated systems, the true utility of this table is in its index of the underlying depth of search and stability grids. These represent more than half of the effort involved in the final determination of the utility of direct imaging of these targets in search for unknown companions. These grids can be combined with updated Doppler completeness values as these become available, in order to produce up to the minute target rankings at the time a mission is launched.

6. CONCLUSIONS

Running numerical simulations up to 10^9 years, we have analyzed and compared various stability criteria for two-planet systems with arbitrary eccentricities, showing that the criterion from Petrovich (2015) is generally the most conservative and useful for our purposes, although the stability limits defined by Giuppone et al. (2013) and Petit et al. (2018) also perform reasonably well. The code used to perform the numerical simulations is publicly available at https://github.com/CarlosGascon/NumSim. For any criterion expressed as a boundary of the outer pericenter to inner apocenter ratio (ρ) or the angular momentum deficit (C), we have derived expressions for the conditional probability of having a stable companion given fixed values of a and m. This formulation has been directly used for the computation of analytic stability maps, allowing us to rapidly characterize the stable region of a system in the (a, R) space. By intersecting with the depth-of-search grids defined by Garrett et al. (2017), we have obtained the corresponding stable-imageable region, yielding the definition of the total dynamically stable depth-of-search, with no dependence on the assumed planet population. In particular, we have presented two cases where the detectable region is clearly perturbed by the stability boundaries, showing the importance of accounting for the effects of the existing planet in such systems. Furthermore, we added two examples of systems where the existing planet falls outside the imageable region but its gravitational effect is still noticeable. Finally, the convolution with the selected occurrence grid has allowed us to estimate the expected number of stable and imageable planets in a system. Applying this procedure to all the currently known single-planet systems and several stability criteria, we have built a ranked target

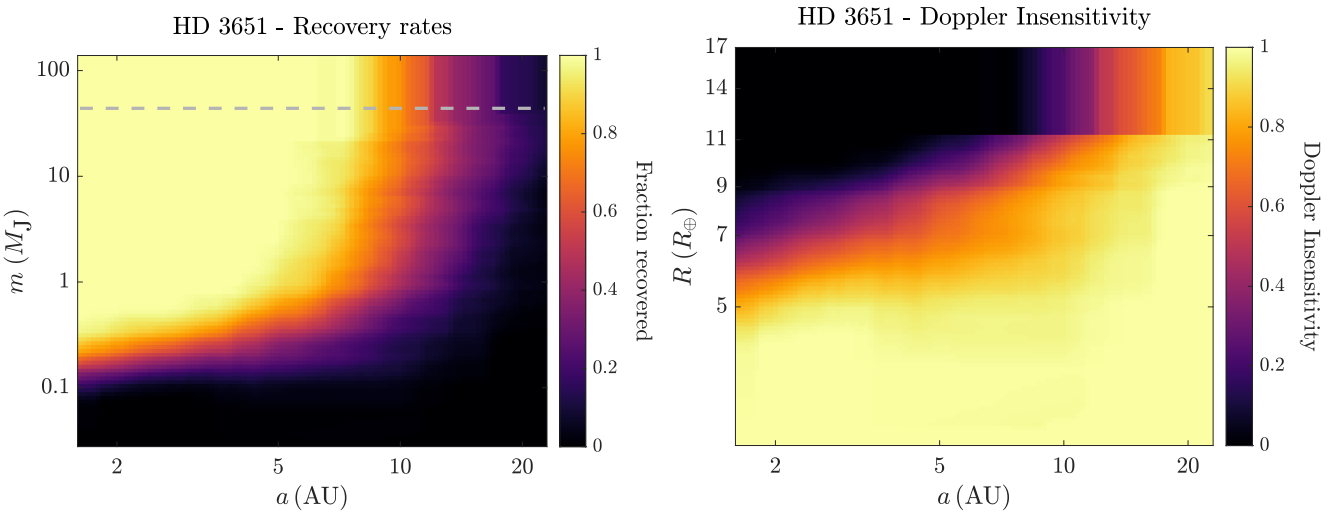

Figure 7. (New Figure) Recovery rates (left) and Doppler insensitivity map (i.e., fraction of non-recovered planets) in the (a, R) space (right) for the system HD 3651. Colour maps were built by translating the results from Howard & Fulton (2016) into our parameter space. In particular, the gray dashed line in the left figure indicates the mass above which the original recovery rates had to be extrapolated following the observed vertical trend.

list based on the **CGI's** capabilities and the SAG13 parametric fit. **Additionally, we have completed our study by considering the radial velocity data from past Doppler surveys and evaluating how the non-detection of additional planets in some of the targets can help us rule out entire regions of our parameter space. Making use of the results from Howard & Fulton (2016), we have observed that the consideration of the radial velocity data reduces significantly the target's total completeness, consequently suggesting that, in future studies, a detailed Doppler analysis for the most interesting targets would be needed in order to improve and complement our prioritization.** The code used for both the construction of analytic stability maps and the systems prioritization is publicly available at https://github.com/CarlosGascon/StableDoS. **The generated depth of search and stability grids are all available via Cornell eCommons at [url to be filled in at time of manuscript acceptance].** Although a numerical analysis could lead to more accurate results, the proposed methodology is a powerful tool, not only for rapidly identifying which targets have a higher probability of hosting an additional planet, but also for discarding those systems where no unknown companions can be detected.

This research made use of the NASA Exoplanet Archive, which is operated by the California Institute of Technology, under contract with the National Aeronautics and Space Administration under the Exoplanet Exploration Program. In addition, this research employed the Imaging Mission Database, which is operated by the Space Imaging and Optical Systems Lab (SIOSlab) at Cornell University. C. G. would also like to thank the Interdisciplinary Higher Education Center (CFIS) from the Polytechnic University of Catalonia (UPC), as well as the CELLEX Foundation, for offering him the opportunity of developing this work at Cornell University.

REFERENCES

Agnew, M. T., Maddison, S. T., & Horner, J. 2018, Monthly Notices of the Royal Astronomical Society, 481, 4680

Batalha, N. E., Smith, A. J., Lewis, N. K., et al. 2018, The Astronomical Journal, 156, 158

Brown, R. A. 2005, The Astrophysical Journal, 624, 1010

Chen, J., & Kipping, D. 2016, The Astrophysical Journal, 834, 17

Deck, K. M., Payne, M., & Holman, M. J. 2013, The Astrophysical Journal, 774, 129

Duncan, M., Quinn, T., & Tremaine, S. 1989, Icarus, 82, 402

Garrett, D., & Savransky, D. 2016, The Astrophysical Journal, 828, 20

Garrett, D., & Savransky, D. 2018, in American Astronomical Society, AAS Meeting, Vol. 231

Garrett, D., Savransky, D., & Macintosh, B. 2017, The Astronomical Journal, 154, 47
Giuppone, C., Morais, M., & Correia, A. 2013, Monthly Notices of the Royal Astronomical Society, 436, 3547
Gladman, B. 1993, Icarus, 106, 247
Hadden, S., & Lithwick, Y. 2018, The Astronomical Journal, 156, 95
Howard, A. W., & Fulton, B. J. 2016, Publications of the Astronomical Society of the Pacific, 128, 114401
Kipping, D. M. 2013, Monthly Notices of the Royal Astronomical Society: Letters, 434, L51
Konopacky, Q. M., Barman, T. S., Macintosh, B. A., & Marois, C. 2013, Science, 339, 1398
Laskar, J. 2000, Physical Review Letters, 84, 3240
Laskar, J., & Petit, A. 2017, Astronomy & Astrophysics, 605, A72
Marchal, C., & Bozis, G. 1982, Celestial Mechanics, 26, 311
Moorhead, A. V., Ford, E. B., Morehead, R. C., et al. 2011, The Astrophysical Journal Supplement Series, 197, 1
Petit, A. C., Laskar, J., & Boué, G. 2017, Astronomy & Astrophysics, 607, A35
Petit, A. C., Laskar, J., & Boué, G. 2018, A&A, 617, A93
Petrovich, C. 2015, The Astrophysical Journal, 808, 120
Rein, H., & Liu, S.-F. 2012, Astronomy & Astrophysics, 537, A128
Wisdom, J. 1980, The Astronomical Journal, 85, 1122

APPENDIX

A. SINGLE-PLANET SYSTEMS RANKING

Table 5. Dynamically stable depth-of-search and completeness values (We would like this table to appear in machine readable format).

Target		Known Planet			Petrovich's Crit.		Giuppone's Crit.		Hill AMD Crit.	
Name	Distance	a_k	e_k	$m_k \sin I$	DoS	Completeness	DoS	Completeness	DoS	Completeness
	(pc)	(AU)		(M_J)	(Dynamically Stable)		(Dynamically Stable)		(Dynamically Stable)	
Proxima Cen	1.30	0.049	0.350	0.004	44.25	0.40553	52.07	0.41418	39.39	0.39538
GJ 411	2.55	0.079	0.220	0.009	52.76	0.36637	57.83	0.37178	45.12	0.35245
Ross 128	3.38	0.050	0.116	0.004	56.37	0.36255	57.89	0.36422	44.41	0.34088
GJ 674	4.55	0.039	0.200	0.035	59.15	0.35824	59.22	0.35833	48.66	0.33925
GJ 687	4.55	0.170	0.040	0.060	54.40	0.35174	59.20	0.35829	46.52	0.33474
GJ 625	6.49	0.078	0.130	0.009	61.58	0.33251	61.90	0.33296	46.38	0.30137
HD 180617	5.91	0.336	0.160	0.038	47.40	0.31868	59.10	0.34149	44.15	0.30944
Gl 686	8.16	0.092	0.077	0.021	62.30	0.30439	62.40	0.30452	45.94	0.27006
GJ 433	9.07	0.060	0.080	0.020	61.39	0.28633	61.40	0.28633	46.17	0.25446
HD 285968	9.47	0.066	0.000	0.026	60.72	0.27940	60.73	0.27941	45.46	0.24692
GJ 436	9.76	0.029	0.138	0.070[b]	61.41	0.27324	61.41	0.27324	53.51	0.25779
Gl 49	9.86	0.091	0.363	0.018	60.91	0.27147	61.07	0.27171	44.00	0.23557
GJ 1265	10.26	0.026	0.040	0.023	61.33	0.26413	61.33	0.26413	49.20	0.23939
GJ 536	10.41	0.067	0.080	0.017	61.58	0.26188	61.59	0.26189	44.52	0.22630
GJ 86	10.79	0.110	0.040	4.420	60.60	0.25471	60.61	0.25473	60.59	0.25467
HD 102365	9.29	0.460	0.340	0.050	46.70	0.25312	60.47	0.28076	42.20	0.24039
HD 147379	10.77	0.323	0.070	0.090	57.24	0.24950	60.68	0.25505	42.53	0.21670
HD 85512	11.28	0.260	0.110	0.010	56.86	0.24182	59.67	0.24641	37.91	0.19858
HD 3651	11.14	0.295	0.645	0.228	49.05	0.22829	60.18	0.24871	42.89	0.19898
GJ 96	11.94	0.291	0.440	0.062	51.30	0.22102	59.49	0.23535	40.27	0.19457
VHS J125601.92-125723.9	12.70	102.0	0.000[a]	11.200	57.47	0.22018	26.42	0.12668	55.94	0.21635
HD 211970	13.00	0.143	0.150	0.041	58.40	0.21789	58.48	0.21803	40.13	0.17971
GJ 3779	13.75	0.026	0.070	0.025	57.74	0.20652	57.74	0.20652	46.62	0.18434
GJ 685	14.32	0.134	0.000	0.028	56.90	0.19775	56.92	0.19778	37.48	0.15788
GJ 1214	14.65	0.014	0.000[a]	0.020[b]	56.25	0.19296	56.25	0.19296	45.87	0.17243
Gl 378	14.96	0.039	0.109	0.041	56.53	0.18869	56.53	0.18869	45.77	0.16756
51 Peg	15.47	0.053	0.013	0.472	55.16	0.18147	55.16	0.18147	54.74	0.18074
HIP 79431	14.54	0.360	0.290	2.100	47.90	0.17905	56.73	0.19474	50.35	0.17237
tau Boo	15.66	0.049	0.011	4.320	55.17	0.17870	55.17	0.17870	55.17	0.17870
HD 177565	16.93	0.246	0.059	0.048	53.47	0.16164	53.54	0.16175	32.83	0.12114
GJ 3942	16.94	0.061	0.121	0.022	53.50	0.16162	53.51	0.16162	36.21	0.12787
GJ 504	17.54	43.50	0.000[a]	4.000	50.98	0.15338	50.44	0.15253	46.06	0.14327
LSPM J2116+0234	17.64	0.088	0.183	0.042	52.71	0.15288	52.72	0.15289	36.69	0.12224

Table 5 continued on next page

Table 5 *(continued)*

Target		Known Planet			Petrovich's Crit.		Giuppone's Crit.		Hill AMD Crit.	
Name	Distance	a_k	e_k	$m_k \sin I$	DoS	Completeness	DoS	Completeness	DoS	Completeness
	(pc)	(AU)		(M_J)	(Dynamically Stable)		(Dynamically Stable)		(Dynamically Stable)	
HN Peg	18.13	773.0	0.000[a]	21.999	51.48	0.14691	51.24	0.14632	51.48	0.14691
HD 99492	18.21	0.120	0.250	0.070	51.17	0.14590	51.21	0.14596	36.75	0.11846
70 Vir	17.91	0.481	0.399	7.416	45.41	0.13822	51.75	0.14952	31.19	0.06767
WD 0806-661	19.20	2500	0.000[a]	7.500	50.01	0.13453	49.77	0.13407	50.01	0.13453
GJ 3021	17.56	0.490	0.511	3.370	41.06	0.13326	52.29	0.15379	31.75	0.07325
HR 810	17.33	0.920	0.140	2.270	39.78	0.13240	52.06	0.15568	41.01	0.13327
HD 192263	19.65	0.150	0.050	0.560	49.38	0.12922	49.39	0.12923	47.09	0.12526
GJ 3634	19.80	0.029	0.080	0.026[b]	49.36	0.12767	49.36	0.12767	36.59	0.10460
HD 104067	20.38	0.260	0.000	0.160	48.34	0.12136	48.41	0.12147	33.65	0.09502
GJ 649	10.38	1.135	0.300	0.328	19.05	0.11665	33.41	0.17755	22.74	0.12044
GJ 4276	21.35	0.082	0.370	0.052	46.58	0.11155	46.59	0.11157	33.42	0.08847
HD 27442	18.28	1.271	0.060	1.560	33.29	0.10893	49.20	0.14089	33.73	0.11127
HD 90156	21.96	0.250	0.310	0.057	45.78	0.10546	45.96	0.10574	25.83	0.07132
HD 4308	22.03	0.120	0.000	0.050	45.71	0.10502	45.71	0.10502	29.56	0.07736
HD 147513	12.91	1.320	0.260	1.210	18.79	0.09736	36.64	0.16028	17.04	0.07235
GJ 3341	23.16	0.089	0.310	0.021	44.18	0.09466	44.18	0.09467	24.63	0.06263
HD 39855	23.28	0.041	0.140	0.027	43.83	0.09364	43.83	0.09364	31.55	0.07342
HIP 12961	23.39	0.250	0.170	0.360	43.40	0.09254	43.49	0.09267	36.19	0.08064
HD 62509	10.34	1.640	0.020	2.300	14.18	0.08797	27.82	0.14986	23.77	0.14131
alf Ari	20.21	1.200	0.250	1.800	29.04	0.08582	46.20	0.11947	30.04	0.08280
HD 156668	24.35	0.050	0.000	0.013	41.73	0.08465	41.73	0.08465	23.46	0.05560
HD 42618	24.35	0.554	0.190	0.045	40.26	0.08238	41.72	0.08465	18.05	0.04721
HD 19994	22.54	1.305	0.063	1.370	31.71	0.07743	44.26	0.09913	28.45	0.07212
HD 16417	25.41	0.140	0.200	0.070	40.37	0.07640	40.37	0.07641	26.21	0.05474
alf Tau	20.43	1.460	0.100	6.470	23.19	0.06815	44.02	0.11328	31.05	0.08371
HD 103949	26.52	0.439	0.190	0.035	37.92	0.06750	38.51	0.06837	15.20	0.03491
HD 33564	20.97	1.100	0.340	9.100	23.44	0.06595	45.16	0.11161	22.33	0.04146
HD 210277	21.31	1.130	0.480	1.290	21.57	0.06332	42.77	0.10527	20.89	0.04926
HD 179949	27.48	0.044	0.022	0.916	37.02	0.06204	37.02	0.06204	37.01	0.06204
gam Cep	13.54	2.050	0.049	1.850	11.63	0.05867	24.54	0.11039	19.60	0.09681
HD 125595	28.22	0.080	0.000	0.020	35.59	0.05742	35.59	0.05742	18.03	0.03351
HD 164595	28.28	0.230	0.088	0.051	35.64	0.05703	35.65	0.05704	16.91	0.03172
HD 10647	17.34	2.015	0.150	0.940	14.44	0.05699	29.24	0.10065	19.66	0.07537
HD 93083	28.54	0.477	0.140	0.370	34.77	0.05476	35.31	0.05554	23.95	0.03989
HD 75289	29.14	0.050	0.030	0.490	34.48	0.05209	34.48	0.05209	34.42	0.05201
HD 21411	29.16	0.362	0.400	0.207	34.03	0.05142	34.43	0.05199	21.75	0.03520
HD 102195	29.36	0.050	0.000	0.410	33.97	0.05095	33.97	0.05095	33.87	0.05082
DENIS-P J082303.1-491201	20.77	0.360	0.345	28.500[b]	17.12	0.05088	47.51	0.11737	21.82	0.03981

Table 5 continued on next page

Table 5 *(continued)*

Target		Known Planet			Petrovich's Crit.		Giuppone's Crit.		Hill AMD Crit.	
Name	Distance	a_k	e_k	$m_k \sin I$	DoS	Completeness	DoS	Completeness	DoS	Completeness
	(pc)	(AU)		(M_J)	(Dynamically Stable)		(Dynamically Stable)		(Dynamically Stable)	
GJ 3470	29.45	0.036	0.000[a]	0.044[b]	33.75	0.05047	33.75	0.05047	26.41	0.04063
HD 46375	29.58	0.040	0.063	0.226	33.59	0.04972	33.59	0.04972	33.32	0.04935
HD 101930	30.05	0.300	0.110	0.250	32.88	0.04722	32.94	0.04731	23.67	0.03529
HD 52265	30.01	0.520	0.270	1.210	32.53	0.04681	33.04	0.04751	29.59	0.04284
HD 218566	28.85	0.690	0.300	0.200	29.75	0.04656	34.74	0.05377	16.42	0.02951
7 CMa	19.82	1.930	0.220	2.460	13.86	0.04475	31.99	0.09056	15.12	0.04120
HD 162020	30.85	0.080	0.280	9.840	31.45	0.04335	31.45	0.04335	31.40	0.04323
HD 8326	30.71	0.533	0.200	0.210	31.06	0.04303	31.78	0.04402	16.70	0.02539
HD 128356	26.03	0.870	0.570	0.890	19.22	0.04017	38.84	0.07122	24.53	0.04694
HD 64114	31.55	0.246	0.120	0.056	30.40	0.04010	30.41	0.04011	13.48	0.02021
HD 130322	31.91	0.093	0.029	1.150	29.96	0.03848	29.96	0.03849	29.94	0.03846
HIP 71135	32.36	0.335	0.210	0.059	28.97	0.03642	29.08	0.03656	11.31	0.01658
HIP 35173	33.19	0.217	0.160	0.040	27.96	0.03323	27.97	0.03324	11.01	0.01494
mu Leo	32.63	1.100	0.090	2.400	26.48	0.03232	28.86	0.03546	23.87	0.02925
HD 40979	34.12	0.850	0.250	4.670	24.83	0.02778	26.47	0.02987	25.52	0.02862
HD 45652	34.89	0.237	0.607	0.433	25.25	0.02719	25.32	0.02727	22.62	0.02423
HD 63765	32.57	0.940	0.240	0.530	20.81	0.02498	28.98	0.03568	15.36	0.01996
BD-11 4672	27.30	2.280	0.050	0.530	11.52	0.02441	28.86	0.04998	12.48	0.02800
16 Cyg B	21.15	1.660	0.680	1.780	7.44	0.02285	24.33	0.06426	5.34	0.00867
HD 114386	27.95	1.730	0.230	1.140	11.42	0.02260	31.50	0.05179	15.49	0.02924
HD 216770	36.70	0.460	0.370	0.570	22.18	0.02132	22.65	0.02187	17.91	0.01700
HD 195019	37.71	0.140	0.010	3.980	21.21	0.01928	21.21	0.01928	21.21	0.01928
HD 63454	37.73	0.040	0.000	0.250	21.17	0.01923	21.17	0.01923	21.08	0.01913
HD 117618	37.82	0.180	0.150	0.174	20.98	0.01899	20.99	0.01899	16.18	0.01438
HD 16141	37.83	0.360	0.250	0.260	20.94	0.01894	20.97	0.01897	14.07	0.01248
HD 23079	33.49	1.600	0.100	2.610	16.96	0.01861	27.25	0.03183	18.28	0.02111
HD 111998	33.26	1.820	0.030	4.510	16.75	0.01858	27.42	0.03244	19.26	0.02234
HD 113337	36.22	0.920	0.460	2.830	18.71	0.01770	23.32	0.02320	21.01	0.02045
HD 108147	38.96	0.102	0.530	0.261	19.41	0.01644	19.41	0.01644	18.53	0.01557
2MASS J01225093-2439505	36.00	52.00	0.000[a]	24.500	12.10	0.01626	2.54	0.00413	12.56	0.01697
HD 4208	34.23	1.662	0.042	0.810	15.58	0.01615	26.02	0.02920	10.49	0.01245
HD 102117	39.62	0.150	0.120	0.170	18.57	0.01508	18.57	0.01508	15.14	0.01200
2MASS J02192210-3925225	39.40	156.0	0.000[a]	13.900	16.03	0.01491	1.07	0.00145	13.59	0.01395
GJ 849	8.80	2.350	0.040	1.000	2.11	0.01476	6.51	0.04162	8.14	0.04811
HD 28185	39.43	1.020	0.050	5.900	18.00	0.01449	18.89	0.01545	18.26	0.01480
gam 1 Leo	38.52	1.190	0.144	8.780	17.35	0.01446	19.94	0.01736	19.33	0.01668
HD 114762	40.23	0.360	0.340	10.690	17.68	0.01384	17.74	0.01391	17.70	0.01385

Table 5 continued on next page

Table 5 *(continued)*

Target		Known Planet			Petrovich's Crit.		Giuppone's Crit.		Hill AMD Crit.	
Name	Distance	a_k	e_k	$m_k \sin I$	DoS	Completeness	DoS	Completeness	DoS	Completeness
	(pc)	(AU)		(M_J)	(Dynamically Stable)		(Dynamically Stable)		(Dynamically Stable)	
HD 38283	38.10	1.020	0.410	0.400	16.19	0.01338	20.61	0.01833	8.88	0.00781
HD 111232	28.98	1.970	0.200	7.140	8.24	0.01314	28.55	0.04394	15.50	0.02016
HD 142415	35.57	1.060	0.500	1.670	13.83	0.01269	24.28	0.02504	18.26	0.01827
HD 83443	40.95	0.040	0.010	0.340	16.85	0.01262	16.85	0.01262	16.83	0.01261
HD 178911 B	41.02	0.340	0.110	8.030	16.73	0.01250	16.73	0.01251	16.73	0.01250
HD 98736	32.48	1.864	0.226	2.330	9.52	0.01187	26.59	0.03299	14.86	0.01855
kap CrB	30.09	2.650	0.167	1.811	7.73	0.01176	23.13	0.03227	11.24	0.01784
HD 89744	38.68	0.917	0.677	8.350	14.97	0.01165	19.88	0.01700	18.04	0.01450
HD 103720	41.60	0.050	0.086	0.620	16.08	0.01155	16.08	0.01155	16.08	0.01155
bet UMi	38.78	1.400	0.190	6.100	14.89	0.01153	19.69	0.01677	17.97	0.01495
HD 7199	36.19	1.360	0.190	0.270	13.21	0.01152	23.30	0.02319	6.47	0.00720
HD 168746	41.62	0.070	0.110	0.270	16.05	0.01152	16.05	0.01152	15.81	0.01130
HD 121504	41.71	0.330	0.030	1.510	15.91	0.01138	15.91	0.01138	15.69	0.01117
HD 10697	33.15	2.140	0.104	6.383	10.25	0.01096	25.68	0.03042	16.91	0.01923
HD 197037	33.00	2.070	0.220	0.790	8.95	0.01082	25.09	0.02977	9.41	0.01284
HD 216437	26.71	2.497	0.317	2.223	5.26	0.01078	20.39	0.03537	7.52	0.01112
HD 216435	33.01	2.560	0.070	1.260	9.27	0.01068	23.88	0.02806	9.03	0.01220
HD 6434	42.41	0.140	0.170	0.490	15.02	0.01032	15.02	0.01032	14.71	0.01005
HD 204941	28.74	2.550	0.370	0.230	4.86	0.01021	16.93	0.02538	7.84	0.01662
GJ 179	12.36	2.410	0.210	0.820	1.91	0.01016	6.70	0.03552	3.80	0.01860
HD 85390	33.56	1.373	0.500	0.099	8.04	0.00978	26.31	0.03052	6.17	0.00962
HD 141937	33.39	1.500	0.410	9.690	9.38	0.00970	26.47	0.03104	19.33	0.01926
HD 49674	43.09	0.060	0.090	0.100	14.26	0.00937	14.26	0.00937	12.93	0.00832
HD 137388	40.53	0.890	0.360	0.200	13.01	0.00899	17.31	0.01333	5.17	0.00387
HD 126525	37.69	1.837	0.035	0.237	11.74	0.00896	20.96	0.01911	3.96	0.00421
iot Dra	31.67	1.275	0.712	8.820	6.90	0.00877	28.10	0.03667	20.24	0.02221
HD 208487	44.00	0.524	0.240	0.520	13.22	0.00816	13.27	0.00820	9.89	0.00578
91 Aqr	44.08	0.700	0.027	3.200	13.14	0.00808	13.17	0.00811	12.88	0.00787
HD 42012	36.84	1.670	0.200	1.600	9.16	0.00714	22.02	0.02104	11.56	0.01050
HD 285507	45.09	0.060	0.090	0.980	12.10	0.00699	12.10	0.00699	12.10	0.00699
HD 8574	44.88	0.760	0.300	2.030	12.04	0.00698	12.31	0.00721	11.44	0.00654
30 Ari B	44.71	0.990	0.290	13.820	12.03	0.00696	12.52	0.00739	12.48	0.00735
HD 330075	45.36	0.040	0.000	0.480	11.82	0.00670	11.82	0.00670	11.82	0.00670
HIP 91258	45.95	0.060	0.020	1.090	11.20	0.00612	11.20	0.00612	11.19	0.00612
HD 77338	46.00	0.060	0.090	0.060	11.14	0.00608	11.14	0.00608	8.95	0.00468
HD 114729	37.85	2.067	0.079	0.825	8.61	0.00602	20.36	0.01824	6.17	0.00546
HD 17674	44.48	1.420	0.130	0.870	9.90	0.00523	12.70	0.00765	6.06	0.00317
HD 29021	31.02	2.280	0.459	2.400	3.11	0.00522	18.51	0.02335	6.64	0.00591
BD-17 63	34.49	1.340	0.540	2.850	3.37	0.00520	23.81	0.02595	12.99	0.01150

Table 5 continued on next page

Table 5 *(continued)*

Target		Known Planet			Petrovich's Crit.		Giuppone's Crit.		Hill AMD Crit.	
Name	Distance	a_k	e_k	$m_k \sin I$	DoS	Completeness	DoS	Completeness	DoS	Completeness
	(pc)	(AU)		(M_J)	(Dynamically Stable)		(Dynamically Stable)		(Dynamically Stable)	
HD 70642	29.30	3.318	0.175	1.993	2.99	0.00505	14.53	0.01938	6.06	0.00960
HD 164604	39.41	1.331	0.350	1.998	8.13	0.00496	18.74	0.01538	13.10	0.01006
HD 210193	42.25	1.487	0.240	0.482	9.03	0.00483	15.22	0.01051	4.79	0.00296
HD 30562	26.18	2.340	0.760	1.220	2.38	0.00482	12.25	0.02060	2.37	0.00213
HD 22781	32.63	1.167	0.819	13.650	3.97	0.00449	26.98	0.03284	20.10	0.02080
GU Psc	48.00	2000	0.000[a]	11.300	9.27	0.00442	0.00	0.00000	9.27	0.00442
HR 2562	34.04	20.30	0.000[a]	30.000	2.55	0.00439	2.02	0.00404	5.38	0.00931
HD 154345	18.29	4.210	0.040	0.820	1.43	0.00423	5.21	0.01524	4.91	0.01739
HD 20782	36.02	1.365	0.950	1.488	3.35	0.00401	21.26	0.02067	10.49	0.00813
HD 143105	48.70	0.038	0.070	1.210	8.63	0.00394	8.63	0.00394	8.63	0.00394
HD 89307	32.04	3.270	0.200	2.110	2.68	0.00373	14.68	0.01598	5.72	0.00700
HD 107148	49.49	0.269	0.050	0.210	8.01	0.00344	8.01	0.00344	5.79	0.00233
HD 196885	34.20	2.370	0.480	2.580	2.63	0.00330	17.08	0.01708	7.36	0.00542
WASP-80	49.86	0.034	0.002	0.538[b]	7.69	0.00323	7.69	0.00323	7.69	0.00323
HD 167042	49.73	1.320	0.089	1.700	7.46	0.00307	7.81	0.00330	5.84	0.00226
BD+14 4559	49.42	0.780	0.290	1.040	7.16	0.00288	8.07	0.00348	6.38	0.00257
HD 50554	31.19	2.353	0.501	4.954	1.97	0.00283	16.95	0.02027	7.53	0.00593
HD 81040	34.47	1.940	0.530	7.270	2.71	0.00281	20.06	0.02082	12.91	0.01062
eps Tau	49.23	1.930	0.151	7.600	6.89	0.00270	8.17	0.00359	7.48	0.00315
HD 153950	48.52	1.280	0.340	2.950	6.84	0.00269	8.81	0.00406	7.66	0.00335
HD 100777	49.60	1.030	0.360	1.030	6.42	0.00241	7.90	0.00338	5.49	0.00213
HD 117207	32.38	3.787	0.157	1.926	1.63	0.00223	10.90	0.01051	4.04	0.00535
HD 213240	40.92	1.890	0.420	5.580	4.87	0.00213	16.16	0.01187	12.61	0.00835
HD 32963	38.12	3.410	0.070	0.700	2.16	0.00203	13.41	0.00986	2.56	0.00270
14 Her	17.94	2.930	0.370	4.660	0.55	0.00136	5.33	0.01550	0.80	0.00067
HD 222582	42.21	1.340	0.730	8.370	3.38	0.00117	15.06	0.01034	13.88	0.00912
HD 156846	47.80	1.120	0.850	10.670	3.93	0.00103	9.42	0.00456	9.32	0.00448
HD 187085	45.96	2.100	0.251	0.836	3.53	0.00086	10.95	0.00591	3.24	0.00137
HD 4113	41.92	1.280	0.903	1.560	1.94	0.00081	15.17	0.01060	9.63	0.00589
HD 7449	38.71	2.380	0.920	0.508	0.66	0.00075	8.76	0.00494	1.65	0.00073
HD 70573	45.70	1.760	0.400	6.100	2.91	0.00063	11.27	0.00620	9.58	0.00491
eps Eri	3.21	3.390	0.702	1.550[b]	0.09	0.00046	7.00	0.04020	0.13	0.00016
HD 106252	38.23	2.610	0.480	6.930	0.52	0.00044	11.99	0.00814	7.11	0.00350
HD 142022 A	34.31	2.930	0.530	4.440	0.43	0.00044	9.28	0.00700	3.70	0.00157
HD 171238	44.87	2.570	0.234	2.720	1.30	0.00021	11.00	0.00598	4.65	0.00185
HD 86226	45.74	2.840	0.150	0.920	1.52	0.00020	10.21	0.00525	1.81	0.00060
HD 87883	18.30	3.580	0.530	1.540	0.13	0.00019	1.56	0.00300	0.16	0.00008
psi 1 Dra B	22.16	4.430	0.400	1.530	0.13	0.00016	1.67	0.00217	0.26	0.00017
HD 20868	47.79	0.950	0.750	1.250	1.35	0.00015	9.44	0.00457	6.91	0.00304

Table 5 continued on next page

Table 5 *(continued)*

Target		Known Planet			Petrovich's Crit.		Giuppone's Crit.		Hill AMD Crit.	
Name	Distance	a_k	e_k	$m_k \sin I$	DoS	Completeness	DoS	Completeness	DoS	Completeness
	(pc)	(AU)		(M_J)	(Dynamically Stable)		(Dynamically Stable)		(Dynamically Stable)	
RR Cae	21.20	5.300	0.000	4.200	0.11	0.00013	5.20	0.00761	0.71	0.00133
HD 221420	31.17	18.50	0.420	9.700	0.04	0.00009	1.12	0.00239	0.23	0.00035
HD 220689	46.94	3.396	0.054	1.118	1.04	0.00008	8.62	0.00387	1.10	0.00023
GJ 328	20.54	4.500	0.370	2.300	0.03	0.00003	0.99	0.00120	0.08	0.00003
HD 114613	20.29	5.340	0.458	0.357	0.02	0.00002	0.35	0.00031	0.14	0.00016
HD 45350	46.94	1.920	0.778	1.790	0.15	0.00001	9.00	0.00418	4.85	0.00192
HD 8673	37.90	3.020	0.723	14.200	0.01	0.00001	6.00	0.00253	4.67	0.00144
HD 24040	46.68	4.920	0.040	3.860	0.05	0.00000	4.53	0.00110	0.46	0.00003
DE CVn	30.55	5.750	0.000	12.029[b]	0.00	0.00000	2.40	0.00150	0.08	0.00005
HD 13931	47.46	5.150	0.020	2.200	0.07	0.00000	4.32	0.00100	0.30	0.00001
HD 108341	49.40	2.000	0.850	3.500	0.01	0.00000	6.66	0.00247	4.67	0.00152
HD 79498	49.02	2.980	0.575	1.340	0.00	0.00000	4.94	0.00134	1.46	0.00031
CFBDSIR J145829 +101343	23.10	2.600	0.000[a]	10.500	0.00	0.00000	5.64	0.01107	0.00	0.00000
HD 106515 A	34.12	4.590	0.572	9.610	0.00	0.00000	0.78	0.00014	0.26	0.00001
HIP 70849	24.07	20.25	0.715	9.000	0.00	0.00000	0.00	0.00000	0.00	0.00000
HD 150706	28.29	6.700	0.380	2.710	0.00	0.00000	0.06	0.00001	0.00	0.00000
HD 219077	29.21	6.220	0.770	10.390	0.00	0.00000	0.00	0.00000	0.00	0.00000
HD 25015	37.47	6.190	0.390	4.480	0.00	0.00000	0.13	0.00001	0.00	0.00000
HD 196067	39.98	5.020	0.660	6.900	0.00	0.00000	0.34	0.00002	0.18	0.00000
HD 98649	42.22	6.570	0.860	6.790	0.00	0.00000	0.00	0.00000	0.00	0.00000
HD 13724	43.52	12.40	0.340	26.770	0.00	0.00000	0.00	0.00000	0.00	0.00000
HD 92987	43.59	9.620	0.210	16.880	0.00	0.00000	0.00	0.00000	0.00	0.00000
HD 166724	45.19	5.420	0.734	3.530	0.00	0.00000	0.03	0.00000	0.00	0.00000
HD 133131 B	47.00	6.150	0.610	2.500	0.00	0.00000	0.02	0.00000	0.00	0.00000
HD 181234	47.81	7.520	0.730	8.370	0.00	0.00000	0.00	0.00000	0.00	0.00000
HD 220773	49.00	4.940	0.510	1.450	0.00	0.00000	0.86	0.00003	0.14	0.00000
WISEP J121756.91 +162640.2 A	10.10	8.000	0.000[a]	22.000	0.00	0.00000	0.00	0.00000	0.00	0.00000

[a] The eccentricity of this system's planet was unknown and consequently set to zero.

[b] This system's inclination was known and therefore the given value corresponds to the true mass m_k.

NOTE—Results are obtained for 213 single-planet systems using Petrovich's, Hill AMD and Giuppone's criteria. In particular, the systems are ranked according to the completeness values calculated with Petrovich's criterion.